Versão do arquivo anexado / Version of attached file:

Versão do Editor / Published Version

Mais informações no site da editora / Further information on publisher's website:

https://link.springer.com/article/10.1007/JHEP09(2020)160

DOI: 10.1007/JHEP09(2020)160

Direitos autorais / Publisher's copyright statement:

Constraining the Chiral Magnetic Effect with charge-dependent azimuthal correlations in Pb-Pb collisions at $\sqrt{s_{\mathrm{NN}}} = 2.76$ and $5.02\,\mathrm{TeV}$

The ALICE collaboration

E-mail: ALICE-publications@cern.ch

ABSTRACT: Systematic studies of charge-dependent two- and three-particle correlations in Pb-Pb collisions at $\sqrt{s_{\mathrm{NN}}} = 2.76$ and $5.02\,\mathrm{TeV}$ used to probe the Chiral Magnetic Effect (CME) are presented. These measurements are performed for charged particles in the pseudorapidity (η) and transverse momentum (p_{T}) ranges $|\eta| < 0.8$ and $0.2 < p_{\mathrm{T}} < 5\,\mathrm{GeV}/c$. A significant charge-dependent signal that becomes more pronounced for peripheral collisions is reported for the CME-sensitive correlators $\gamma_{1,1} = \langle\cos(\varphi_\alpha + \varphi_\beta - 2\Psi_2)\rangle$ and $\gamma_{1,-3} = \langle\cos(\varphi_\alpha - 3\varphi_\beta + 2\Psi_2)\rangle$. The results are used to estimate the contribution of background effects, associated with local charge conservation coupled to anisotropic flow modulations, to measurements of the CME. A blast-wave parametrisation that incorporates local charge conservation tuned to reproduce the centrality dependent background effects is not able to fully describe the measured $\gamma_{1,1}$. Finally, the charge and centrality dependence of mixed-harmonics three-particle correlations, of the form $\gamma_{1,2} = \langle\cos(\varphi_\alpha + 2\varphi_\beta - 3\Psi_3)\rangle$, which are insensitive to the CME signal, verify again that background contributions dominate the measurement of $\gamma_{1,1}$.

Contents

1 Introduction

Heavy-ion collisions at ultra-relativistic energies are used to study the phase transition from a deconfined Quark-Gluon Plasma (QGP) state [1–3] to ordinary nuclear matter. The transition is expected to occur at high values of temperature and energy density, which is also supported by quantum chromodynamics (QCD) calculations on the lattice [4, 5]. The main aim of the heavy-ion program at the Large Hadron Collider (LHC) is to study the QGP properties, such as the equation of state, the speed of sound in the medium and the value of the ratio of shear viscosity to entropy density (η/s).

It was soon realised that heavy-ion collisions also allow for studies of novel QCD phenomena associated with parity (P) violation effects in strong interactions [6, 7]. These effects are catalysed by the presence of a strong magnetic field that develops in the early stages of heavy-ion collisions. This field is created by the motion of the charged nucleons of the incoming ions in a non-central collision, i.e. a collision with a large impact parameter, defined as the distance between the centers of the two colliding nuclei in the transverse plane. The magnitude of this field can reach values of 10^{18} Gauss [8], making it the strongest magnetic field created by any experiment on earth. The direction of the magnetic field is along the system's angular momentum and perpendicular to the reaction plane. The latter is the plane defined by the impact parameter vector and the beam direction.

The potential to observe parity violation in the strong interaction using ultra-relativistic heavy-ion collisions has first been discussed in refs. [9–11] and was further reviewed in refs. [12, 13]. In QCD, this symmetry violation originates from the possibility that the QGP can carry net chirality [14–16], characterised by a non-zero value of the axial chemical potential μ_5, i.e. reflecting the imbalance between left– and right-handed fermions in the system. Depending on the sign of μ_5 the QGP will have an excess of either left– ($\mu_5 < 0$) or right-handed ($\mu_5 > 0$) (anti-)quarks. In the presence of the strong magnetic field, the spins of (anti-)quarks tend to align along the direction of the field, creating a spin polarisation effect. This in turn leads to the development of a vector current along the direction of the magnetic field and the creation of an electric dipole moment of QCD matter. The experimental search for these effects has intensified lately, following the realisation that the subsequent creation of charged hadrons results in an experimentally accessible charge separation along the direction of this magnetic field, and perpendicular to the reaction plane. This phenomenon is called the Chiral Magnetic Effect (CME) and its existence was recently reported in semimetals like zirconium pentatelluride ($ZrTe_5$) [17].

The resulting charge separation can be identified by studying the P-odd sine terms in the Fourier decomposition of the particle azimuthal distribution [18] according to

$$\frac{dN}{d\varphi_\alpha} \sim 1 + 2\sum_n \left[v_{n,\alpha} \cos(n\Delta\varphi_\alpha) + a_{n,\alpha} \sin(n\Delta\varphi_\alpha) \right], \tag{1.1}$$

where $\Delta\varphi_\alpha = \varphi_\alpha - \Psi_{RP}$ is the azimuthal angle φ_α of the particle of type α (either positively or negatively charged particles) relative to the reaction plane angle Ψ_{RP}. The coefficient $v_{n,\alpha}$ is the n-th order Fourier harmonic, averaged over all events, and characterises the anisotropies in momentum space. The reaction plane is not an experimental observable but can be approximated by the second-order symmetry plane, Ψ_2, determined by the direction of the beam and the axis of the maximal particle density in the elliptic azimuthal anisotropy. This symmetry plane and more generally the plane angles of different order Ψ_n, estimated in each event, are introduced to account for the event-by-event fluctuations in the initial energy density of a heavy-ion collision [19–23]. In case of a smooth distribution of matter produced in the overlap zone, the angle Ψ_2 coincides with that of the reaction plane, i.e. $\Psi_2 = \Psi_{RP}$. The leading order P-odd coefficient $a_{1,\alpha}$ reflects the magnitude of the effects from local parity violation, while higher orders ($a_{n,\alpha}$ for $n > 1$) describe the specific shape in azimuth. However, the chiral imbalance that leads to the creation of the CME changes from event to event and the event average $\langle a_{1,\alpha}\rangle$ will be consistent with zero. Consequently, the effect can be detected only by correlation studies.

In ref. [24], it was suggested that a suitable way to probe the CME is via a two-particle correlation technique relative to the second-order symmetry plane of the form $\langle \cos(\varphi_\alpha + \varphi_\beta - 2\Psi_2)\rangle$, where the brackets indicate an average over all events. Here, α and β denote particles with the same or opposite electric charge. The advantage of using this expression is that it probes correlations between two leading order P-odd coefficients $a_{1,\alpha}$ and $a_{1,\beta}$ which do not trivially average to 0 over all events (see section 3 for the discussion). In addition, the observable is constructed as the difference between correlations in- and out-of plane which is expected to significantly suppress parity-conserving background effects. In

order to independently evaluate the contributions from correlations in- and out-of plane one measures at the same time a two-particle correlator of the form $\langle \cos(\varphi_\alpha - \varphi_\beta) \rangle$. Section 3 contains a detailed discussion about all these correlators.

Experimental results for charged particles in both Pb-Pb collisions at $\sqrt{s_{NN}} = 2.76\,\text{TeV}$ at the LHC [25] and in Au-Au collisions up to $\sqrt{s_{NN}} = 0.2\,\text{TeV}$ at the Relativistic Heavy-Ion Collider (RHIC) [26–30] are consistent with the expectation for a charge separation relative to the reaction plane due to the existence of parity violating effects. However, these measurements could be dominated by background effects whose sources have not been fully quantified yet. One of the first attempts to provide a quantitative estimate of the background in the measurement of the CME sensitive correlator (i.e. $\langle \cos(\varphi_\alpha + \varphi_\beta - 2\Psi_2) \rangle$) identified the sources as originating from local charge conservation coupled to the elliptic flow modulation quantified by v_2 [31, 32]. Therefore, the challenge is to define a way to constrain and quantify the background, while in parallel isolating the signal that comes from the CME.

A first step in this direction was taken by the ALICE Collaboration [33] using a method proposed and developed in ref. [34]. This method, called Event Shape Engineering (ESE), utilises the fluctuations of the initial geometry and selects events with different initial system shapes, e.g. central Pb-Pb collisions with large initial anisotropy. This study set an upper limit of 26-33% at 95% confidence level for the CME signal contribution to the $\langle \cos(\varphi_\alpha + \varphi_\beta - 2\Psi_2) \rangle$) correlator in the 10–50% centrality interval. The CMS [35] and the STAR [36] collaborations studied charge-dependent correlations in p-Pb collisions at $\sqrt{s_{NN}} = 5.02\,\text{TeV}$ and in p-Au and d-Au collisions at $\sqrt{s_{NN}} = 0.2\,\text{TeV}$, respectively. In these colliding systems, one expects the CME contribution to any charge-dependent signal to be small and the results can thus be used to gauge the magnitude of the background in heavy-ion collisions. Both results illustrate that these correlations are similar to those measured in heavy-ion collisions. First results using ESE have been reported by the CMS Collaboration in ref. [37], which set upper limits on the CME fraction of the three-particle correlator to be 13% and 7% (at 95% confidence level) for p-Pb and Pb-Pb collisions.

In this article we report results on two-particle correlations of different orders as well as various two-particle correlations relative to the second, third and fourth-order symmetry planes for charged particles in Pb-Pb collisions at $\sqrt{s_{NN}} = 2.76$ and $5.02\,\text{TeV}$. The motivation for utilising different planes is that the charge separation originating from the CME is expected to be present along the direction of the magnetic field and thus perpendicular to the reaction plane, approximated by Ψ_2. Since the third order symmetry plane Ψ_3 is very weakly correlated with Ψ_2 [38] the charge separation effect relative to the third harmonic symmetry plane is expected to be negligible. First results on correlations relative to Ψ_3 reported by the CMS collaboration in ref. [37] indicates that the charge separation could be originating from the coupling of two-particle correlations with the anisotropic flow. In addition, contributions from correlations induced by the CME should be strongly suppressed in the measurements of two-particle correlations relative to Ψ_4, while the background effects stemming from local charge conservation should scale with v_4 [39]. Therefore, measurements of correlations relative to higher order symmetry planes are expected to reflect mainly, if not solely, background effects.

The article is organised as follows: section 2 describes briefly the experimental setup, while section 3 discusses the data sample, the selection criteria as well as the correlators reported; these sections are followed by section 4 and section 5 where the estimation of the systematic uncertainties of all measurements and the main physics results, respectively, are presented. We conclude in section 6 with a summary.

2 Experimental setup

By convention in ALICE, the beam direction defines the z-axis, the x-axis is horizontal and points towards the centre of the LHC, and the y-axis is vertical and points upwards. The apparatus consists of a set of detectors located in the central barrel, positioned inside a solenoidal magnet which can generate a field parallel to the beam direction with maximum magnitude of 0.5 T. A set of forward detectors completes the experimental setup.

The main tracking devices of ALICE are the Inner Tracking System (ITS) [40] and the Time Projection Chamber (TPC) [41]. The ITS consists of six cylindrical layers of silicon detectors employing three different technologies. The two innermost layers, positioned at $r = 3.9$ cm and 7.6 cm, are Silicon Pixel Detectors (SPD), followed by two layers of Silicon Drift Detectors (SDD) ($r = 15$ cm and 23.9 cm). Finally, the two outermost layers are double-sided Silicon Strip Detectors (SSD) at $r = 38$ cm and 43 cm. The TPC surrounds the ITS and provides full azimuthal coverage. The combined pseudorapidity (η) coverage of the ITS and the TPC is $-0.9 < \eta < 0.9$.

A set of forward detectors, the V0 scintillator arrays [42], were used in the trigger logic and for the determination of the collision centrality, discussed in the next section. The V0 consists of two sub-systems, the V0A and the V0C, that are positioned on either side of the interaction point and cover the pseudorapidity ranges of $2.8 < \eta < 5.1$ and $-3.7 < \eta < -1.7$, respectively. Finally the Zero Degree Calorimeters (ZDC) [40] positioned at both positive and negative rapidity at around 114 m away from the interaction point were also used offline to reduce the contamination from beam-induced background.

A detailed description of ALICE and its sub-detectors can be found in ref. [40] and their performance in ref. [43].

3 Analysis details

3.1 Event and track selection

The analysis is performed using the Pb-Pb data samples collected in 2010 and 2015 at a centre-of-mass energy per nucleon pair of $\sqrt{s_{\mathrm{NN}}} = 2.76$ and 5.02 TeV, respectively. The minimum bias trigger condition is defined in the 2010 data sample by combinations of hits in the SPD and either V0A or V0C detectors, while in 2015 the trigger required a signal in both V0A and V0C detectors.

An offline event selection relying on the timing information from the V0 and the neutron ZDC is used to reject beam-gas background and parasitic beam-beam interactions. Events are analysed if the z-coordinate of the reconstructed primary vertex (V_z) resides within ± 10 cm from the nominal interaction point. The collision centrality is estimated from the amplitude of the signal measured by the V0 detectors as explained in

ref. [44]. Higher amplitude, and hence higher particle multiplicity, corresponds to more central (smaller impact parameter) events. The data sample is divided into centrality classes which span 0–70% of the inelastic hadronic cross section, which is considered in this study. The 0–5% and 60–70% intervals correspond to the most central and the most peripheral collisions, respectively.

Charged particles reconstructed using the TPC and the ITS information are accepted for analysis within η and p_{T} ranges of $|\eta| < 0.8$ and $0.2 < p_{\mathrm{T}} < 5\,\mathrm{GeV}/c$, respectively. The tracking algorithm, based on the Kalman filter [45, 46], starts from a collection of space points (referred to as clusters) inside the TPC, and provides the quality of the fit by calculating its χ^2 value. The track parameters at the primary vertex are then updated using the combined information from both the TPC and the ITS detectors. Tracks are accepted even if the algorithm is unable to match the track reconstructed in the TPC with associated SPD clusters (e.g. due to inefficiencies caused by dead channels in the SPD layers). In this case, a cluster from another layer of the ITS (e.g. SDD) is used to reconstruct the tracks. This tracking mode will be referred to as hybrid tracking in the rest of the text and is used as the default in this analysis since it provides a uniform distribution in azimuthal angle (φ). More details about the tracking parameters and performance are described elsewhere [40, 43]. Accepted tracks are required to have at least 70 out of 159 possible space points measured in the TPC and a χ^2 per degree of freedom of the momentum fit per TPC cluster to be below 2. These selections reduce the contribution from short tracks, which are unlikely to originate from the primary vertex. To further reduce the contamination by secondary tracks from weak decays or from the interaction with the material, only tracks within a maximum distance of closest approach (DCA) to primary vertex in both the transverse plane ($\mathrm{DCA_{xy}} < 2.4$ cm) and the longitudinal direction ($\mathrm{DCA_z} < 3.2$ cm) were considered. Moreover, if matched to ITS clusters, the tracks are required to have at least one cluster in either of the two SPD layers. These selections lead to an efficiency of about 65% for primary tracks at $p_{\mathrm{T}} = 0.5\,\mathrm{GeV}/c$, which reaches 80% above $1\,\mathrm{GeV}/c$. The variation of these values between central and peripheral collisions is less than 3%, and does not change between $\sqrt{s_{\mathrm{NN}}} = 2.76$ and $5.02\,\mathrm{TeV}$. The contamination from secondaries is about 10% at $p_{\mathrm{T}} = 0.2\,\mathrm{GeV}/c$, reaches 5% at $p_{\mathrm{T}} = 1\,\mathrm{GeV}/c$ and decreases further with increasing transverse momentum.

3.2 Analysis methodology

A way to probe the P-odd leading order coefficient $a_{1,\alpha}$ that reflects the magnitude of the CME is through the study of charge-dependent two-particle correlations relative to the reaction plane Ψ_{RP}. The expression proposed in ref. [24] is of the form $\langle \cos(\varphi_\alpha + \varphi_\beta - 2\Psi_{\mathrm{RP}}) \rangle$ (α and β being particles with the same or opposite charges) that can probe correlations between the leading P-odd terms for different charge combinations $\langle a_{1,\alpha} a_{1,\beta} \rangle$. This can be seen if one decomposes the correlator using eq. (1.1)

$$
\begin{aligned}
\langle \cos(\varphi_\alpha + \varphi_\beta - 2\Psi_{\mathrm{RP}}) \rangle &= \langle \cos\left[(\varphi_\alpha - \Psi_{\mathrm{RP}}) + (\varphi_\beta - \Psi_{\mathrm{RP}})\right] \rangle \\
&= \langle \cos(\Delta\varphi_\alpha + \Delta\varphi_\beta) \rangle \\
&= \langle \cos\Delta\varphi_\alpha \cos\Delta\varphi_\beta \rangle - \langle \sin\Delta\varphi_\alpha \sin\Delta\varphi_\beta \rangle \\
&= \langle v_{1,\alpha} v_{1,\beta} \rangle + \mathrm{B_{in}} - \langle a_{1,\alpha} a_{1,\beta} \rangle - \mathrm{B_{out}}, \quad (3.1)
\end{aligned}
$$

where B_{in} and B_{out} represent the parity-conserving correlations projected onto the in- and out-of-plane directions. The terms $\langle\cos\Delta\varphi_\alpha\cos\Delta\varphi_\beta\rangle$ and $\langle\sin\Delta\varphi_\alpha\sin\Delta\varphi_\beta\rangle$ in eq. (3.1) quantify the correlations with respect to the in- and out-of-plane directions, respectively. The term $\langle v_{1,\alpha}v_{1,\beta}\rangle$, i.e. the product of the first order Fourier harmonics or directed flow, is expected to have negligible charge dependence in the midrapidity region [47]. In addition, for a symmetric collision system the average directed flow at midrapidity is zero. A generalised form of eq. (3.1) also describing higher harmonics is given by the mixed-harmonics correlations, which reads

$$\gamma_{m,n} = \langle\cos(m\varphi_\alpha + n\varphi_\beta - (m+n)\Psi_{|m+n|})\rangle, \tag{3.2}$$

where m and n are integers. Setting m = 1 and n = 1 (i.e. $\gamma_{1,1}$) leads to eq. (3.1). The $|m+n|$-th order symmetry plane angle $\Psi_{|m+n|}$ is introduced to take into account that the overlap region of the colliding nuclei exhibits an irregular shape [19–23]. This originates from the initial density profile of nucleons participating in the collision, which is not isotropic and differs from one event to the other. In case of a smooth distribution of matter produced in the overlap zone, the angle $\Psi_{|m+n|}$ coincides with that of the reaction plane, i.e. $\Psi_{|m+n|} = \Psi_{RP}$.

In order to independently evaluate the contributions from correlations in- and out-of-plane, one can also measure a two-particle correlator of the form

$$\begin{aligned}
\langle\cos(\varphi_\alpha - \varphi_\beta)\rangle &= \langle\cos\left[(\varphi_\alpha - \Psi_{RP}) - (\varphi_\beta - \Psi_{RP})\right]\rangle \\
&= \langle\cos(\Delta\varphi_\alpha - \Delta\varphi_\beta)\rangle \\
&= \langle\cos\Delta\varphi_\alpha\cos\Delta\varphi_\beta\rangle + \langle\sin\Delta\varphi_\alpha\sin\Delta\varphi_\beta\rangle \\
&= \langle v_{1,\alpha}v_{1,\beta}\rangle + B_{in} + \langle a_{1,\alpha}a_{1,\beta}\rangle + B_{out},
\end{aligned} \tag{3.3}$$

which corresponds to the special case of m = −n in eq. (3.2). This provides access to the two-particle correlations without any dependence on the symmetry plane angle

$$\delta_m = \langle\cos[m(\varphi_\alpha - \varphi_\beta)]\rangle. \tag{3.4}$$

This correlator, owing to its construction, is affected if not dominated by non-flow contributions. Charge-dependent results for δ_1, together with the relevant measurements of $\gamma_{1,1}$ were first reported in ref. [25] and made it possible to separately quantify the magnitude of correlations in- and out-of-plane.

In this article, we report on the charge-dependent results of four correlators of the form of eq. (3.2). The first two, $\gamma_{1,1}$ and $\gamma_{1,-3}$, probe correlations of particles relative to the second order symmetry plane (Ψ_2). The correlator $\gamma_{1,1}$ (i.e. the main correlator used in previous studies) probes correlations of the first order P-odd term, i.e. $\langle a_{1,\alpha}a_{1,\beta}\rangle$ as illustrated in eq. (3.1), while the second is sensitive not only to the first but also the third order coefficient, i.e. $\langle a_{1,\alpha}a_{3,\beta}\rangle$ and thus is sensitive to the magnitude and the shape of the CME contribution. However, in both cases the background contributions from local charge conservation are expected to be significant (see refs. [31, 32] and the references therein).

In order to evaluate the background, correlations relative to the third and fourth order symmetry planes i.e., $\gamma_{1,2}$ and $\gamma_{2,2}$, are investigated. Since the charge-separation effects

originating from the CME form relative to the second order symmetry plane, both correlators are expected to have negligible contribution from it. Their charge-dependent part could thus be used as a proxy for the background that consists of local charge conservation scaled by the corresponding flow harmonics according to ref. [48]

$$\gamma_{1,1} \approx \langle \cos[(\varphi_\alpha - \varphi_\beta) + 2(\varphi_\beta - \Psi_2)] \rangle \propto \delta_1 v_2, \tag{3.5a}$$

$$\gamma_{1,2} \approx \langle \cos[(\varphi_\alpha - \varphi_\beta) + 3(\varphi_\beta - \Psi_3)] \rangle \propto \delta_1 v_3, \tag{3.5b}$$

$$\gamma_{2,2} \approx \langle \cos[2(\varphi_\alpha - \varphi_\beta) + 4(\varphi_\beta - \Psi_4)] \rangle \propto \delta_2 v_4. \tag{3.5c}$$

By taking the difference of results between opposite- and same-sign charge combinations, denoted as $\Delta\gamma_{mn}$ in the most general form of the correlator, one can eliminate the charge-independent part and probe the contribution from local charge conservation modulated by the relevant flow harmonic

$$\Delta\gamma_{1,1} \approx \kappa_2 v_2 \Delta\delta_1, \tag{3.6a}$$

$$\Delta\gamma_{1,2} \approx \kappa_3 v_3 \Delta\delta_1, \tag{3.6b}$$

$$\Delta\gamma_{2,2} \approx \kappa_4 v_4 \Delta\delta_2, \tag{3.6c}$$

where κ_n is a proportionality constant. Using eqs. (3.6), one can thus estimate the contribution of the background in the charge-dependent CME sensitive correlator $\Delta\gamma_{1,1}$ using the results of e.g. $\Delta\gamma_{1,2}$ according to

$$\Delta\gamma_{1,1}^{\mathrm{Bkg}} \approx \Delta\gamma_{1,2} \times \frac{v_2}{v_3}\frac{\kappa_2}{\kappa_3}. \tag{3.7}$$

Equation (3.7) serves as a tool to disentangle the CME contribution from the background, provided the parameter κ_2/κ_3 is estimated. In ref. [35] it was argued that the magnitude of these κ_n terms depends on the kinematic ranges (e.g. detector acceptance, event and particle selection criteria). Although κ_n may have dependency on p_{T} and η, we have ignored such dependency and assumed a constant magnitude of the ratio κ_2/κ_3 for the full kinematic range. In ref. [35], it was suggested that one can assume that $\kappa_2 \approx \kappa_3$ if the same kinematic conditions are used to calculate $\Delta\gamma_{m,n}$ within the same experimental setup. In this article, we also investigate the relationship between κ_2 and κ_3 using two approaches: a blast wave [49] inspired model that incorporates effects of local charge conservation and the results of A Multi Phase Transport model (AMPT) [50–52], both discussed in detail in the Results section.

3.2.1   The event-plane method

To evaluate the correlations experimentally, the event-plane method [53, 54] is used. In this method, the event plane angle is reconstructed from the azimuthal distribution of the particles produced in a collision. The event plane angle of k-th order (where k = |m − n|) $\Psi_{\mathrm{k,EP}}$ is estimated according to

$$\Psi_{\mathrm{k,EP}} = \tan^{-1}\frac{Q_{\mathrm{k,y}}}{Q_{\mathrm{k,x}}}, \tag{3.8}$$

where $Q_{\mathrm{k,x}}$ and $Q_{\mathrm{k,y}}$ are the x- and y-components of the Q-vector, calculated as

$$Q_{\mathrm{k,x}} = \sum_{i=1}^{M} w_i(p_{\mathrm{T}}, \eta, \varphi, V_z) \cos(\mathrm{k}\varphi_i), \text{ and } Q_{\mathrm{k,y}} = \sum_{i=1}^{M} w_i(p_{\mathrm{T}}, \eta, \varphi, V_z) \sin(\mathrm{k}\varphi_i). \qquad (3.9)$$

In eq. (3.9), φ_i corresponds to the azimuthal angle of the i-th track in an event with multiplicity M. The factors $w_i(p_{\mathrm{T}}, \eta, \varphi, V_z)$ are weights applied on every track in the construction of the Q-vectors, in order to correct for non-uniform reconstruction efficiency and acceptance. They are calculated as a function of the transverse momentum, pseudorapidity and azimuthal angle of particles for different V_z values of the primary vertex.

To reduce the contributions from short range effects not related to the common symmetry planes (i.e. non-flow), a subevent plane technique [53, 54] is implemented. Each event is divided into two subevents "A" and "B", covering the ranges $-0.8 < \eta < 0$ and $0 < \eta < 0.8$, respectively, and the two subevent plane angles, namely $\Psi_{\mathrm{k},A}$ and $\Psi_{\mathrm{k},B}$ are calculated using charged particles. The correlators of eq. (3.2) are then calculated as

$$\gamma_{\mathrm{mn}} = \frac{\langle \cos[\mathrm{m}\varphi_\alpha + \mathrm{n}\varphi_\beta - (\mathrm{m} + \mathrm{n})\Psi_{|\mathrm{m+n}|,\mathrm{EP}}] \rangle}{R(\Psi_{|\mathrm{m+n}|,\mathrm{EP}})}, \qquad (3.10)$$

where α and β correspond to any two charged particles within $-0.8 < \eta < 0.8$, and $\Psi_{|\mathrm{m+n}|,\mathrm{EP}}$ corresponds to subevent plane $\Psi_{\mathrm{k},A}$ (or $\Psi_{\mathrm{k},B}$ for systematic studies). Particles α or β (or both) were excluded from the determination of event plane if they were from the same η window as the one used to calculate $\Psi_{\mathrm{k},A}$ or $\Psi_{\mathrm{k},B}$.

The event plane resolution $R(\Psi_{|\mathrm{m+n}|,\mathrm{EP}})$ is given by

$$R(\Psi_{|\mathrm{m+n}|,\mathrm{EP}}) = \sqrt{\cos[|\mathrm{m} + \mathrm{n}|(\Psi_{|\mathrm{m+n}|,A} - \Psi_{|\mathrm{m+n}|,B})]}. \qquad (3.11)$$

The amount of non-flow correlations in the results of both same- (SS) and opposite-sign (OS) charge combinations could also depend on the longitudinal position of the detector used for the estimation of Ψ_k. However, it was checked that the charge-dependent differences, i.e. OS-SS are not affected by this choice as these non-flow contributions (approximately) cancel out in the subtraction.

4 Systematic uncertainties

The systematic uncertainties in all measurements presented in this article were estimated by varying the event and track selection criteria as well as by studying the detector effects with Monte Carlo (MC) simulations. The contributions from different sources, described below, were extracted from the difference for the results of each correlator obtained with the primary selection criteria and the ones after the relevant variation was applied. All sources with a difference between the results larger than 1σ were then added in quadrature to form the final value of the systematic uncertainty (for each data point), where σ is the uncertainty of the difference between the default results and the ones obtained from the variation of the selection criteria, taking into account the degree of their correlation [55].

(No.) Source	Default Value	Variations
(1) Primary V_z	± 10 cm	± 8 cm
(2) Centrality Estimator	V0 amplitude	SPD cluster
(3) Magnetic field polarity	Combined	Positive, Negative
(4) Event plane	$\Psi_{\mathrm{k},-0.8<\eta<0}$	$\Psi_{\mathrm{k},0<\eta<0.8}$
(5) Residual Pile-Up	High Intensity data	Low Intensity data
(6) TPC space points	70	100
(7) DCA_{xy} (DCA_z)	2.4 (3.2) cm	2.0 (2.0) cm
(8) Tracking Algorithm	Hybrid	Global
(9) Charge Combination	" $++$ " and " $--$ " combined	" $++$ " or " $--$ "

Table 1. List of the selection criteria and the corresponding variations used for the estimation of the systematic uncertainties.

Table 1 summarises the sources and the variations that were tested. In particular, the systematic uncertainty originating from the selection of the z position of the primary vertex was investigated by changing this selection from ± 10 cm down to ± 8 cm. In order to estimate the contribution to the results from the choice of the detector used as centrality estimator, the analysis was performed using the number of hits in the second layer of the SPD instead of the amplitude of the V0 detector. Furthermore, data samples recorded with different magnetic field configurations for the solenoid magnet were analysed separately. The contribution of residual pile-up events to the results was estimated by analysing independently the high and low interaction rate samples. Finally, the results were obtained separately by calculating the event plane from different pseudorapidity ranges within the TPC acceptance. The systematic uncertainty in the extraction of the CME fraction when using different event plane angles within the TPC acceptance for the highest LHC energy was estimated considering runs with low beam intensity where the distortions in the TPC are negligible.

In parallel, to investigate any potential bias originating from the quality of the tracks used in the analysis, the number of space points measured in the TPC was varied from 70 (default) up to 100 out of 159 maximum points that a track can have. The contribution stemming from secondary tracks, either from weak decays or from the interaction of particles with the detector material, was investigated by tightening the selection on the DCA in the longitudinal direction as well as in the transverse plane. Finally, another tracking mode that relies on the combination of the TPC and the ITS detectors, henceforth called global tracking, with tighter selection criteria in addition to requirements for clusters in the SPD or the SDD detectors was used. In this case, a stricter transverse momentum dependent requirement in the value of the DCA in the transverse plane resulted in reducing even further the amount of secondary particles in the track sample. The resulting contamination from secondaries is less than 2–3% for the entire p_{T} range.

For each variation, new correction maps for detector inefficiencies and non-uniform acceptance were extracted using MC data samples and collision data.

Sources	$\gamma_{1,1}$ ($\times 10^{-5}$)			$\gamma_{1,2}$ ($\times 10^{-5}$)			$\gamma_{1,-3}$ ($\times 10^{-5}$)			$\gamma_{2,2}$ ($\times 10^{-5}$)		
	SS	OS	OS-SS	SS	OS	OS-SS	SS	OS	OS-SS	SS	OS	OS-SS
(1)	0.26	1.4	0.027	1.1	0.12	1.9	0.13	0.15	0.095	0.035	0.1	0.02
(2)	2.5	6.1	6	4.5	9.9	1.8	4.2	3.2	1.2	8.6	8.6	0.27
(3)	0.86	0.65	0.1	0.83	0.84	0.024	0.34	0.54	0.04	1.4	0.98	0.36
(4)	1.62	1.81	1.6	1.7	1.83	4.51	0.86	0.64	0.15	1.78	2.1	6.8
(5)	4.0	3.9	0.58	7.2	3.9	3.6	0.73	0.83	0.2	4.4	4.0	11
(6)	0.1	0.89	0.065	1.1	1.4	1.3	0.21	0.22	0.032	4.1	3.9	0.12
(7)	0.011	0.032	0.001	0.05	0.06	2.1	0.008	0.024	0.025	0.017	0.28	0.03
(8)	0.045	0.049	0.16	0.67	1.3	0.08	0.07	0.06	0.17	5.7	0.17	0.1
(9)	0.55	—	0.55	0.26	—	0.26	0.23	—	0.23	21	—	21

Table 2. Maximum systematic uncertainty (absolute value) over all centrality intervals on $\gamma_{\rm mn}$ from individual sources (see table 1 for an explanation of each source). The ranges are similar for both energies.

Tables 2 and 3 summarise the maximum magnitude, over all centrality intervals, of the systematic uncertainties from each individual source for all correlators presented in this article. The uncertainties are reported separately for the results for same-sign (SS), opposite-sign (OS) and the difference between opposite- and same-sign (OS-SS) pairs. The uncertainties for the results of the various $\gamma_{m,n}$ are reported without the common factor of $\times 10^{-5}$.

Throughout the centrality intervals reported in this article, the magnitude of $\gamma_{1,1}$ correlator varies between -2.4 to -40 for SS pair, -1.2 to 29 for OS pair and 1.2 to 68 for OS-SS. The values of $\gamma_{1,-3}$ vary between -2.1 to 38 for SS pair, -0.67 to 68 for OS pair and 1.4 to 30 for OS-SS. The magnitude of $\gamma_{1,2}$ covers the range between -2.5 to 140 for SS pair, -1.7 to 180 for OS pair and 0.71 to 3.7 for OS-SS. Finally, the results for $\gamma_{2,2}$ vary between 0.01 to 14.7 for SS and OS pair while being between 0.25 and 19 for OS-SS.

The two-particle correlators of the form δ_m are an order of magnitude larger than the three-particle correlators. Therefore, the values mentioned in the following have an exponent of $\times 10^{-4}$. The magnitude of δ_1 varies between 2.9 to 23.5 for SS pair, 5.6 to 49 for OS pair and 2.7 to 26.2 for OS-SS. The values of δ_2 spans the range between 8.2 to 97 for SS pair, 9.5 to 102 for OS pair and 1.31 to 5.2 for OS-SS. The magnitude of δ_3 varies between 4.5 to 16 for SS pair, 4.8 to 15 for OS pair and -1.3 to 0.79 for OS-SS. Finally, the results for δ_4 varies between 1.58 to 9.4 for SS pair, 1.6 to 6.8 for OS pair and -2.5 to 0.78 for OS-SS.

5   Results

The measurements of two-particle correlators (eq. (3.4)) are presented in figure 1. Each data point on this figure and in the rest of the article is drawn with the relevant statistical (vertical lines) and systematic uncertainties (shaded boxes).The plots in the left panel of figure 1 present the centrality dependence of $\delta_{\rm m}$ for m = 1, 2, 3 and 4 for opposite (OS) and same (SS) sign pairs. The charge-dependent differences of every correlator, denoted

Sources	δ_1 ($\times 10^{-4}$)			δ_2 ($\times 10^{-4}$)			δ_3 ($\times 10^{-4}$)			δ_4 ($\times 10^{-4}$)		
	SS	OS	OS-SS	SS	OS	OS-SS	SS	OS	OS-SS	SS	OS	OS-SS
(1)	1.7	1.8	0.01	0.12	0.13	0.03	0.08	0.11	0.03	0.06	0.05	0.01
(2)	2.0	3.6	1.6	0.65	0.66	0.019	0.5	0.11	0.34	0.43	0.17	0.27
(3)	0.86	1.0	0.35	1.6	1.4	0.25	0.64	0.22	0.33	0.52	0.02	0.51
(5)	1.2	0.91	1.5	1.4	0.99	0.029	0.89	0.38	0.33	0.61	0.13	0.022
(6)	0.014	2.2	1.4	5.5	5.5	1.1	0.26	1.1	1.1	0.94	2.2	0.12
(7)	0.056	0.15	0.01	0.08	0.14	0.01	0.05	0.02	0.02	0.14	0.02	0.07
(8)	2.5	1.8	0.74	0.92	0.29	1.2	1.2	0.53	1.8	0.68	0.67	1.4
(9)	2.6	—	2.6	1.6	—	1.6	1.7	—	1.7	0.37	—	0.37

Table 3. Maximum systematic uncertainty (absolute value) over all centrality intervals on δ_{m} from individual sources (see table 1 for an explanation of each source). The ranges are similar for both energies.

by $\Delta\delta_1$, $\Delta\delta_2$, $\Delta\delta_3$, and $\Delta\delta_4$ as a function of collision centrality are presented in the right panel of figure 1. These charge-dependent two-particle correlators (eq. (3.4)) are primarily dominated by background effects (see discussion in section 3) and can thus be used to constrain the background in the CME sensitive correlator $\gamma_{1,1}$. The first harmonic correlator, δ_1, exhibits a significant charge-dependent difference. This correlator is related to the balance function also studied at the LHC [56, 57]. The present results are qualitatively consistent with the ones in refs. [56] and [57], i.e. oppositely charged particles are more tightly correlated in central events resulting in a narrowing of the balance function width in $\Delta\varphi$ and thus in a smaller value of δ_1 for central events compared to peripheral Pb-Pb collisions. For higher harmonics, the charge-dependent differences become progressively smaller and are compatible with zero (up to centrality $\leq 60\%$) with a hint of negative $\Delta\delta_4$ for the most peripheral events.

The two-particle correlators were also studied in a more differential way, namely as a function of the transverse momentum difference $\Delta p_{\mathrm{T}} = |p_{\mathrm{T},\alpha} - p_{\mathrm{T},\beta}|$, the average transverse momentum $\overline{p}_{\mathrm{T}} = (p_{\mathrm{T},\alpha} + p_{\mathrm{T},\beta})/2$ and the pseudorapidity difference $\Delta\eta = |\eta_\alpha - \eta_\beta|$ of the pair.

The dependence of δ_1, δ_2, δ_3 and δ_4 on these variables for one indicative centrality interval (30–40%) is shown in figure 2 for Pb-Pb collisions at $\sqrt{s_{\mathrm{NN}}} = 5.02\,\mathrm{TeV}$. For the first harmonic correlator, δ_1, the correlations between particles of opposite charges have larger magnitude compared with the ones for same charge particles. The absolute differences do not show any significant Δp_{T} dependence, however they do increase with increasing $\overline{p}_{\mathrm{T}}$ of the pair. Finally, there is a significant charge-dependent difference of δ_1, which decreases with increasing $\Delta\eta$, consistent with what is also reported in refs. [56, 57]. For higher harmonics, no significant difference is observed. For other centralities the results look qualitatively similar.

The measurements of integrated two-particle correlators relative to various order symmetry planes (eq. (3.2)) in Pb-Pb collisions at $\sqrt{s_{\mathrm{NN}}} = 5.02\,\mathrm{TeV}$ are presented in figure 3.
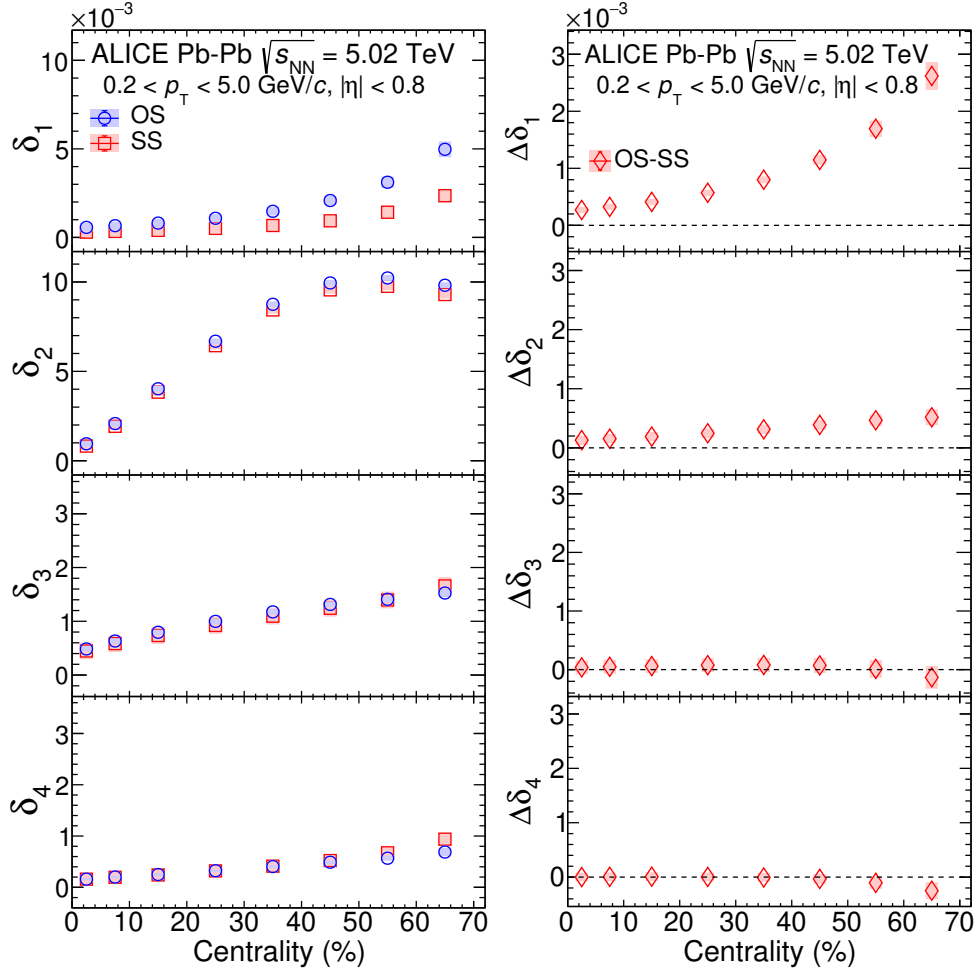
Figure 1. (Left panel) The centrality dependence of δ_1, δ_2, δ_3, and δ_4 for pairs of particles of opposite (OS) and same (SS) sign measured in Pb-Pb collisions at $\sqrt{s_{\mathrm{NN}}} = 5.02\,\mathrm{TeV}$. (Right panel) The charge-dependent differences, $\Delta\delta_{\mathrm{n}}$ for $n = 1, 2, 3$ and 4, as a function of collision centrality. The statistical uncertainties for some data points are smaller than the marker size. The systematic uncertainties of each data point are represented by the shaded boxes.

The left panel presents the centrality dependence of $\gamma_{1,1}$, $\gamma_{1,-3}$, $\gamma_{1,2}$ and $\gamma_{2,2}$. Results for different charge combinations, i.e. OS and SS pairs are also presented here. The right panel of the same figure presents the centrality dependence of the charge-dependent differences, i.e. OS-SS. A significant charge-dependent magnitude for $\gamma_{1,1}$ is observed that increases when moving to more peripheral collisions. In particular, the magnitude of the same-sign correlations becomes progressively more negative, while correlations of oppositely charged particles are very close to zero and their magnitude turns positive for peripheral Pb-Pb events. A significant charge-dependent difference that increases for peripheral centrality intervals is also observed for $\gamma_{1,-3}$. Both correlators, as discussed in section 3, probe correlations between either the first order P-odd term of the form $\langle a_{1,\alpha} a_{1,\beta} \rangle$ or between the first and the third order coefficient $\langle a_{1,\alpha} a_{3,\beta} \rangle$. They are thus sensitive to contributions from the CME.
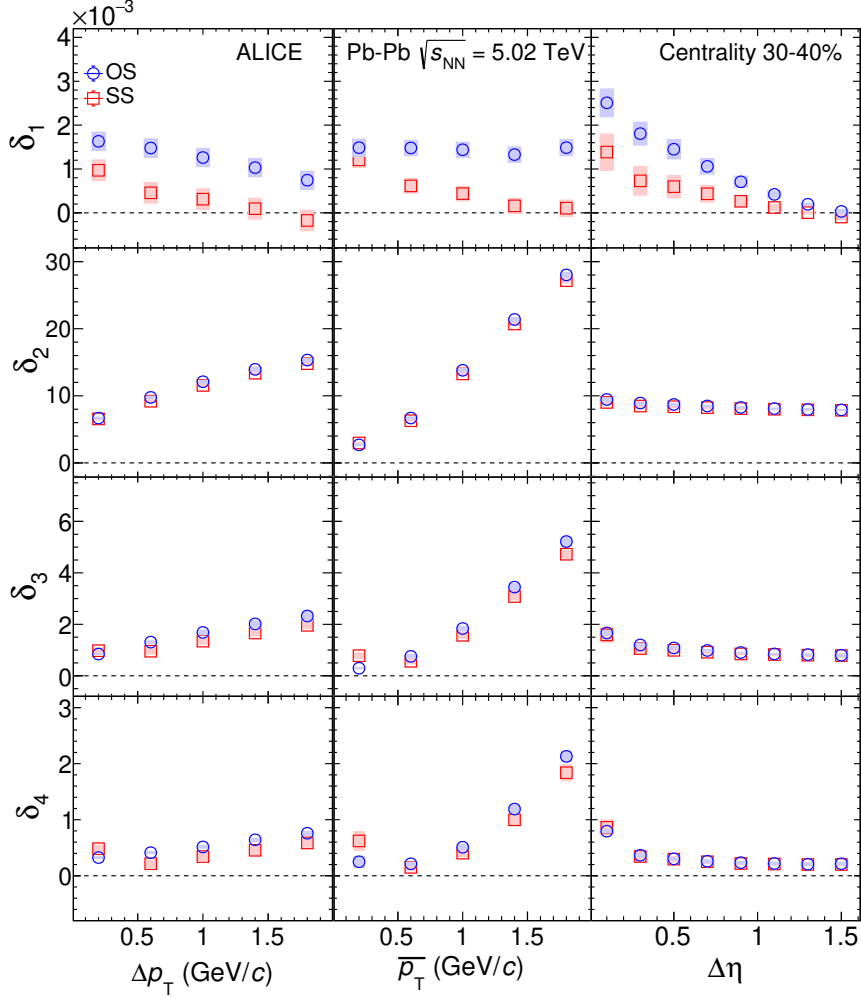
Figure 2. The dependence of δ_1, δ_2, δ_3 and δ_4 on the transverse momentum difference $\Delta p_{\mathrm{T}} = |p_{\mathrm{T},\alpha} - p_{\mathrm{T},\beta}|$ (left panel), the average transverse momentum $\bar{p}_{\mathrm{T}} = (p_{\mathrm{T},\alpha} + p_{\mathrm{T},\beta})/2$ (middle panel) and the pseudorapidity difference $\Delta\eta = |\eta_\alpha - \eta_\beta|$ (right panel) of the pair. The results for both opposite (circles) and same sign (squares) particle pairs are reported for one indicative centrality interval (30–40%) of Pb-Pb collisions at $\sqrt{s_{\mathrm{NN}}} = 5.02\,\mathrm{TeV}$.

The centrality dependence of $\gamma_{1,2}$ for SS and OS pairs and their difference also demonstrate a significant charge dependence which increases for more peripheral events. Correlations of particles relative to the third order symmetry plane are expected to probe solely the background scaled by the third order flow harmonic (v_3) as expressed in eqs. (3.5). Hence these results indicate that the effects of local charge conservation coupled with v_3 can induce differences in correlations between different charges. Finally, correlations of particles with different charge relative to the fourth order symmetry plane, as quantified by $\gamma_{2,2}$, do not exhibit any significant charge dependence within the current level of statistical and systematic uncertainties.

As in the case of the two-particle correlators, δ_{m}, also the $\gamma_{\mathrm{m,n}}$ were studied in a differential way, namely as a function of Δp_{T}, $\bar{p}_{\mathrm{T}}$ and $\Delta\eta$. The results are presented in
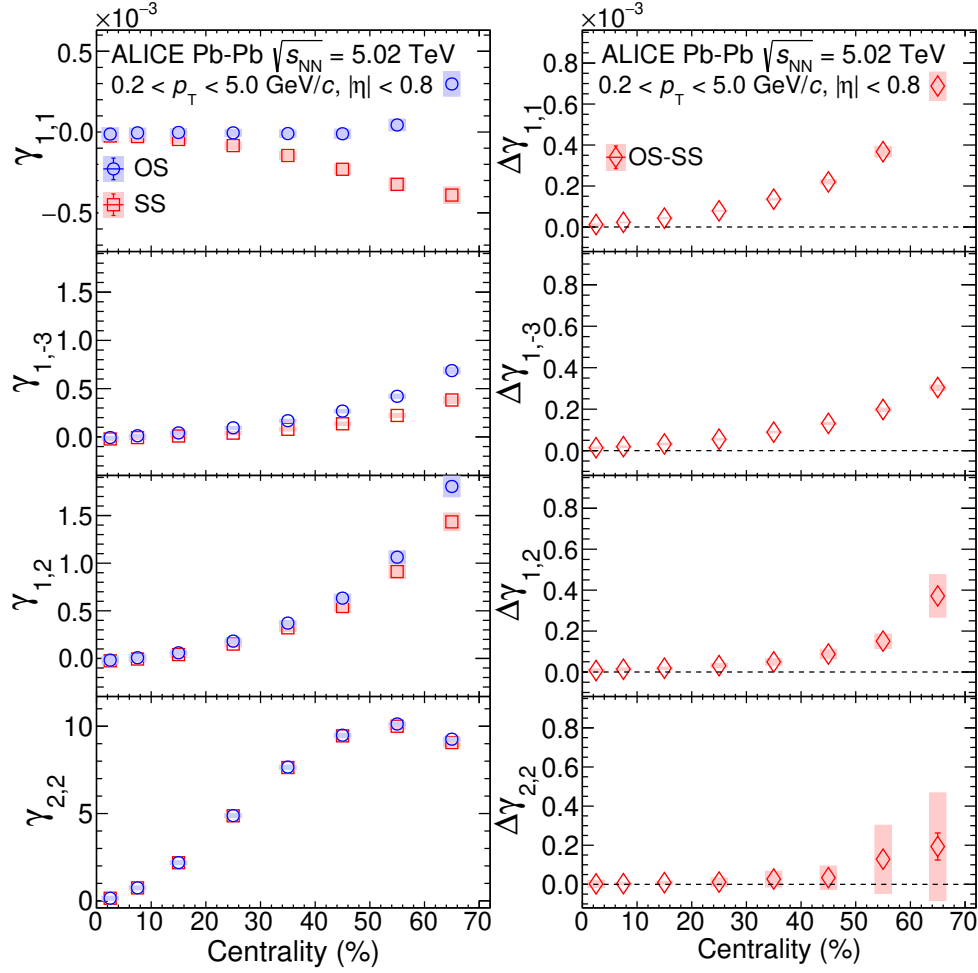
Figure 3. Left panel: the centrality dependence of $\gamma_{1,1}$, $\gamma_{1,-3}$, $\gamma_{1,2}$ and $\gamma_{2,2}$ for pairs of particles of opposite (OS) and same (SS) sign measured in Pb-Pb collisions at $\sqrt{s_{\mathrm{NN}}} = 5.02\,\mathrm{TeV}$. (Right panel): the charge-dependent differences $\Delta\gamma_{1,1}$, $\Delta\gamma_{1,-3}$, $\Delta\gamma_{1,2}$ and $\Delta\gamma_{2,2}$ as a function of collision centrality.

figure 4 for the same representative centrality interval as before (30–40%) for both OS and SS. It is seen that, with the exception of $\gamma_{2,2}$, the magnitude of correlations for OS pairs is greater than the one of SS for nearly the full range of Δp_{T}, $\overline{p}_{\mathrm{T}}$ and $\Delta\eta$ presented in this article. The results for OS and SS are compatible within the current level of statistical and systematic uncertainties for $\gamma_{2,2}$.

The correlations of particles with different charge for both $\gamma_{1,1}$ and $\gamma_{1,-3}$, i.e. the two correlators that are sensitive to different orders of the CME, have a range that extends up to one unit of $\Delta\eta$. Both OS and SS correlations have a similar trend as a function of Δp_{T} and $\Delta\eta$, however they exhibit different behaviour as a function of $\overline{p}_{\mathrm{T}}$. On the other hand, the correlators that are solely sensitive to the background, i.e. $\gamma_{1,2}$ and $\gamma_{2,2}$, exhibit an increasing trend as a function of both Δp_{T} and $\overline{p}_{\mathrm{T}}$. This trend has a mild charge dependence for $\gamma_{1,2}$ that increases with increasing Δp_{T} and $\overline{p}_{\mathrm{T}}$, but not for $\gamma_{2,2}$. Both $\gamma_{1,2}$ and $\gamma_{2,2}$ have a range that extends up to $\Delta\eta = 1.6$ without any significant dependence on $\Delta\eta$.
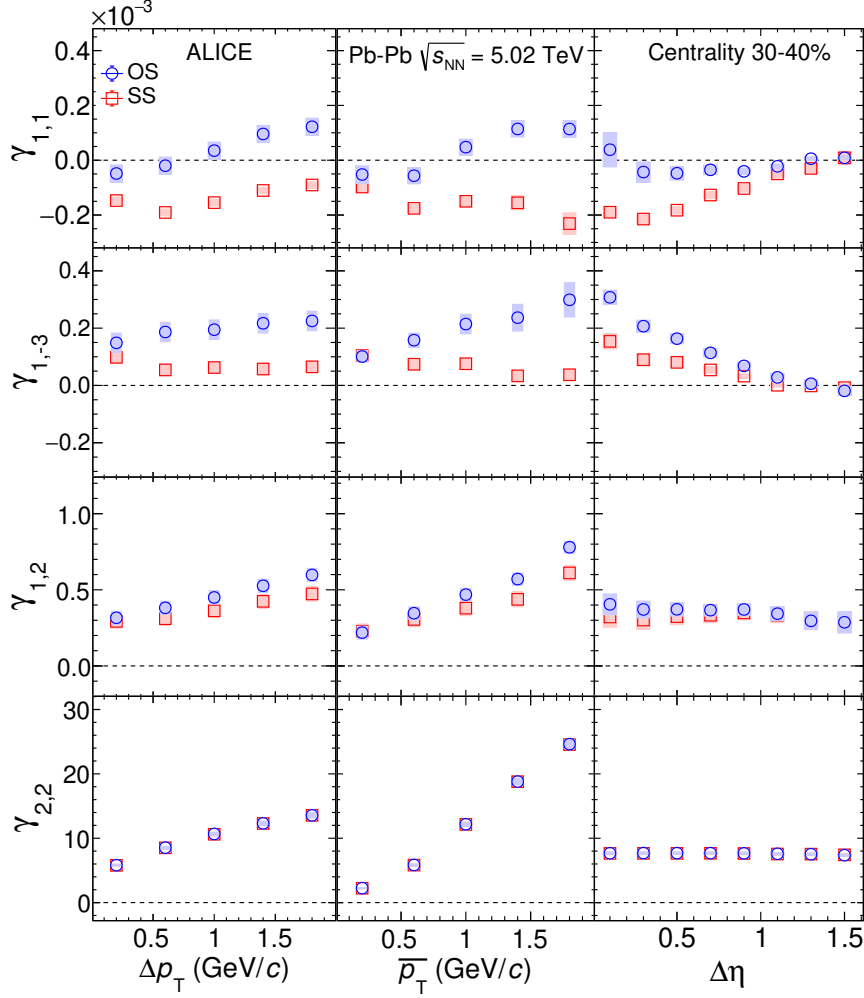
Figure 4. The dependence of $\gamma_{1,1}$, $\gamma_{1,-3}$, $\gamma_{1,2}$ and $\gamma_{2,2}$ on the transverse momentum difference $\Delta p_{\mathrm{T}} = |p_{\mathrm{T},\alpha} - p_{\mathrm{T},\beta}|$ (left panel), the average transverse momentum $\overline{p}_{\mathrm{T}} = (p_{\mathrm{T},\alpha} + p_{\mathrm{T},\beta})/2$ (middle panel) and the pseudorapidity difference $\Delta\eta = |\eta_\alpha - \eta_\beta|$ (right panel) of the pair. The results for both opposite and same sign particle pairs are reported for one indicative centrality interval (30–40%) of Pb-Pb collisions at $\sqrt{s_{\mathrm{NN}}} = 5.02\,\mathrm{TeV}$.

Finally, the charge-dependent differences of the correlators $\gamma_{1,1}$, $\gamma_{1,2}$ and $\gamma_{2,2}$ were also studied in Pb-Pb collisions at $\sqrt{s_{\mathrm{NN}}} = 2.76\,\mathrm{TeV}$. The centrality dependence of $\Delta\gamma_{1,1}$, $\Delta\gamma_{1,2}$ and $\Delta\gamma_{2,2}$ is presented in figure 5 in comparison with the results obtained in Pb-Pb collisions at $\sqrt{s_{\mathrm{NN}}} = 5.02\,\mathrm{TeV}$. None of the correlators exhibit any significant differences between the two energies, within the current level of uncertainties. This could be explained considering that there is no significant energy dependence in the effects that constitute the background to these measurements (i.e. local charge conservation coupled to different flow harmonic modulations). Preliminary studies indicate that the correlations between balancing charges, as reflected in the width of the balance function, do not exhibit any significant dependence on collision energy. The values of v_2, v_3 and v_4 in $\sqrt{s_{\mathrm{NN}}} = 5.02\,\mathrm{TeV}$ are between 2 to 20% higher than the values at $\sqrt{s_{\mathrm{NN}}} = 2.76\,\mathrm{TeV}$ [58]. However, the
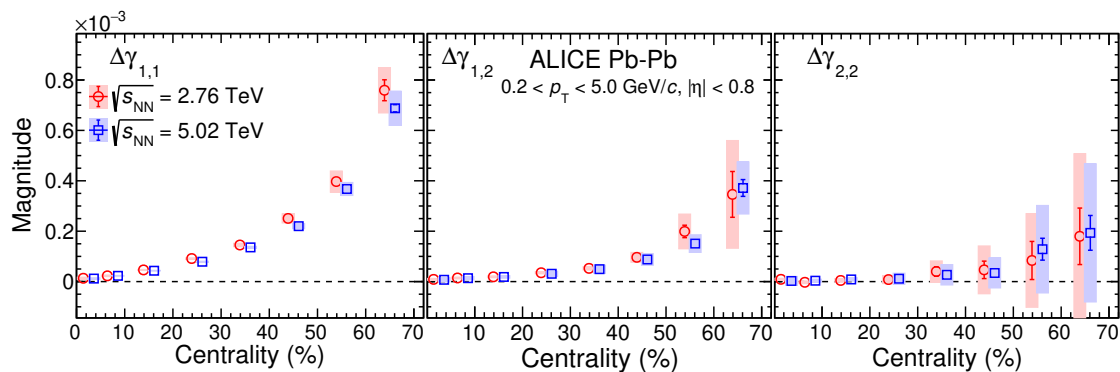
Figure 5. The dependence of $\Delta\gamma_{1,1}$, $\Delta\gamma_{1,2}$ and $\Delta\gamma_{2,2}$ on centrality, measured in Pb-Pb collisions at $\sqrt{s_{\mathrm{NN}}} = 2.76$ and $5.02\,\mathrm{TeV}$. The data points for $\sqrt{s_{\mathrm{NN}}} = 5.02\,\mathrm{TeV}$ are shifted along the horizontal axis for better visibility.

Centrality	T_{kin} (MeV)	ρ_0	ρ_2	R_x/R_y
0–5%	91.3 ± 3.5	1.26 ± 0.01	0.020 ± 0.001	0.956 ± 0.001
5–10%	87.0 ± 3.5	1.27 ± 0.01	0.032 ± 0.001	0.933 ± 0.002
10–20%	84.8 ± 4.9	1.25 ± 0.01	0.045 ± 0.003	0.905 ± 0.004
20–30%	87.4 ± 4.8	1.23 ± 0.01	0.059 ± 0.007	0.872 ± 0.005
30–40%	91.6 ± 3.8	1.20 ± 0.01	0.068 ± 0.003	0.844 ± 0.004
40–50%	95.1 ± 3.3	1.15 ± 0.01	0.070 ± 0.003	0.823 ± 0.004
50–60%	98.1 ± 3.2	1.09 ± 0.01	0.065 ± 0.002	0.807 ± 0.004
60–70%	108.0 ± 3.2	0.99 ± 0.01	0.056 ± 0.002	0.786 ± 0.006

Table 4. List of the Blast-wave fit parameters.

corresponding change in the background contribution to the $\gamma_{\mathrm{m,n}}$ correlator is of the order of a few percent, which is not distinguishable within the current level of uncertainties.

5.1 Constraining the CME contribution

5.1.1 Describing the background with Blast-wave inspired LCC model

As a first approach to constraining the CME contribution, a blast-wave (BW) parametrisation [49] that describes the phase space density at kinetic freeze-out, is used. This model assumes that the radial expansion velocity is proportional to the distance from the centre of the system and takes into account resonance production and decays. Local charge conservation (LCC) is additionally incorporated in this model by generating ensembles of particles with zero net charge. The position of the sources of balancing charges are then uniformly distributed within an ellipse. From now on this model will be denoted as BW-LCC in the text.

Each particle of an ensemble is emitted by a fluid element with a common collective velocity following the single-particle BW parametrisation. The procedure starts from obtaining BW parameters by fitting the p_{T} spectra [59] and the p_{T}-differential v_2 values [60] for charged pions, kaons, and protons (antiprotons) measured in Pb-Pb collisions
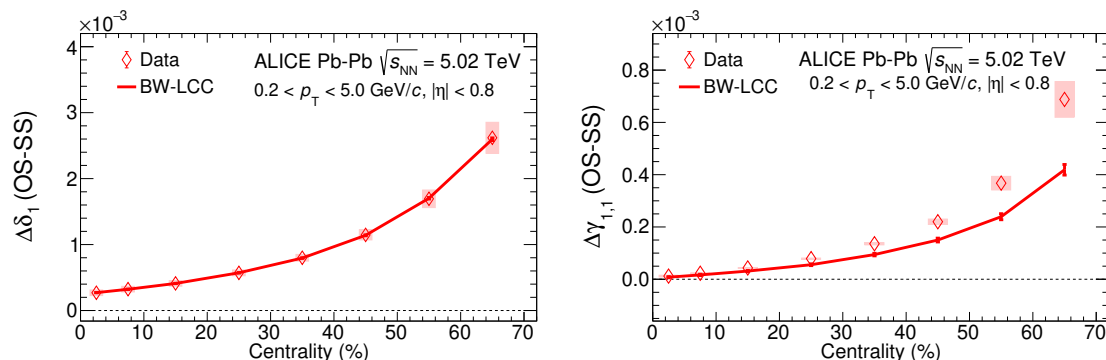
Figure 6. (Left) The centrality dependence of $\Delta\delta_1$ measured in Pb-Pb collisions at $\sqrt{s_{NN}} = 5.02$ TeV. The curve (denoted as BW-LCC) presents the blast-wave parametrization coupled to local charge conservation effects. The model is tuned to reproduce the measured values of $\Delta\delta_1$ (see text for details). (Right) The comparison of the centrality dependence of the CME-sensitive correlator $\Delta\gamma_{1,1}$ with expectations from the BW-LCC model.

at $\sqrt{s_{NN}} = 5.02$ TeV. The fit ranges for p_T spectra are $0.5 \leq p_T \leq 1.0$ GeV/c, $0.2 \leq p_T \leq 1.5$ GeV/c and $0.2 \leq p_T \leq 3.0$ GeV/c for pions, kaons and protons, respectively. The fit range for p_T-differential v_2 and v_4 is $0.5 \leq p_T \leq 1.2$ GeV/c. Table 4 presents the resulting BW parameters, namely the kinetic freezeout temperature (T_{kin}), radial flow (ρ_0) and its second order modulation (ρ_2) as well as the spacial asymmetry (R_x/R_y). The next step required tuning the number of sources of balancing pairs for each centrality interval to reproduce the centrality dependence of $\Delta\delta_1$, the correlator which is mainly sensitive to background effects. This procedure is repeated for every centrality interval. The number of sources varies from ~2476 to 193 for the centrality intervals 0–5% to 60–70%. The left panel of figure 6 presents the agreement achieved between the measured results and the ones obtained from the model. Overall the model describes the measurement fairly well with deviations limited to <1% for the whole centrality range. The tuned model is then used to extract the expectation for the centrality dependence of the charge-dependent differences of the CME sensitive correlator $\Delta\gamma_{1,1}$. The right panel of figure 6 shows the comparison between the measured values of $\Delta\gamma_{1,1}$ and estimates from the model. The estimate of $\Delta\gamma_{1,1}$ from the model originates solely from the contribution of local charge conservation effects coupled to elliptic flow modulations. The curve underestimates the measured data points by as much as $\approx 39\%$, with the disagreement increasing progressively for more peripheral events.

5.1.2 Describing the background with v_n and $\gamma_{m,n}$

In the following, we attempt to constrain the background contribution to the CME sensitive correlator $\gamma_{1,1}$ and thus give an estimation of the fraction of the signal in Pb-Pb collisions. The approach described in section 3.2 relies on the assumption that the coefficients κ_n have similar magnitude, allowing one to calculate the background contribution to $\Delta\gamma_{1,1}$, denoted as $\Delta\gamma_{1,1}^{Bkg}$ from $\Delta\gamma_{1,2}$ according to eq. (3.7). This assumption was tested using events produced with the string melting tune of A Multi Phase Transport model (AMPT) [50–52].
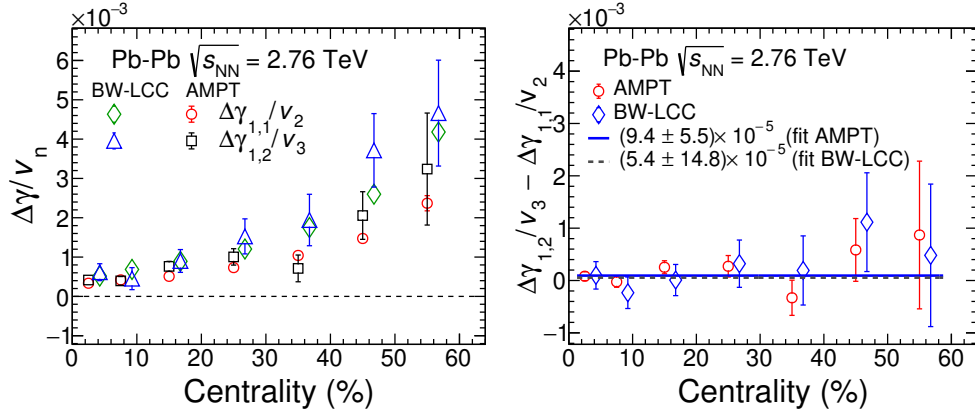
Figure 7. (Left panel) The centrality dependence of $\Delta\gamma_{1,1}/v_2$ and $\Delta\gamma_{1,2}/v_3$ for Pb-Pb collisions at $\sqrt{s_{NN}} = 2.76$ TeV according to the AMPT and BW-LCC model. (Right panel) The differences between $\Delta\gamma_{1,1}/v_2$ and $\Delta\gamma_{1,2}/v_3$ in AMPT and BW-LCC, denoted as $\Delta(\Delta\gamma/v_n)$. The solid and dotted line is the result of a fit with a constant function to AMPT and BW-LCC result respectively.

In the string melting tune, the initial strings are melted into partons whose interactions are described by a parton cascade model [61]. These partons are then combined into final-state hadrons via a quark coalescence model. In this model, the final-state hadronic rescattering is implemented including resonance decays as well. The input parameters $\alpha_s = 0.33$ and a partonic cross section of 1.5 mb were used to reproduce the centrality dependence of v_2 and v_3 for charged particles, as reported in ref. [62], for Pb-Pb events at $\sqrt{s_{NN}} = 2.76$ TeV. About 40 million simulated Pb-Pb events were analysed, split into centrality based on the values of the impact parameter. Only primary particles having the same kinematic selections as in the experimental data (i.e. $|\eta| < 0.8$ and $0.2 < p_T < 5$ GeV/c) were considered. The left panel of figure 7 presents the ratio of the charge-dependent differences $\Delta\gamma_{1,1}$ and $\Delta\gamma_{1,2}$ to the relevant harmonics v_2 and v_3, respectively. Similar ratios are also shown from the BW-LCC model, which is discussed in the previous subsection. The two sets of data points are compatible within uncertainties over the entire centrality range for both AMPT and BW-LCC model. This is also illustrated in the right panel of figure 7, which presents the centrality dependence of $(\Delta\gamma_{1,1}/v_2) - (\Delta\gamma_{1,2}/v_3)$, denoted as $\Delta(\Delta\gamma/v_n)$. The corresponding data points from AMPT and BW-LCC are fitted with a constant function, which yields a result compatible with zero within the uncertainties of the fit i.e., $\Delta(\Delta\gamma/v_n) = (9.4 \pm 5.5) \times 10^{-5}$ and $(5.4 \pm 14.8) \times 10^{-5}$ respectively. This observation illustrates that within these models one can assume $\kappa_2 \approx \kappa_3$. Results presented in this article have been also reproduced using the AMPT version reported in [63].

The same procedure was used with Pb-Pb data recorded at both LHC energies. Since the results of $\gamma_{2,2}$ do not give any significant charge-dependent difference as a function of centrality within statistical and systematic uncertainties (see figure 3), only the values of $\gamma_{1,2}$ are used in the rest of the article to estimate the background.

Although, CME sensitive $\gamma_{1,-3}$ correlator could have similar dependence on the background as $\gamma_{1,1}$ (i.e., $\gamma_{1,-3} \propto \delta_1 v_2$), we observe in figure 3 that their magnitude are not the same. This difference, which is being investigated as part a of future publication, makes
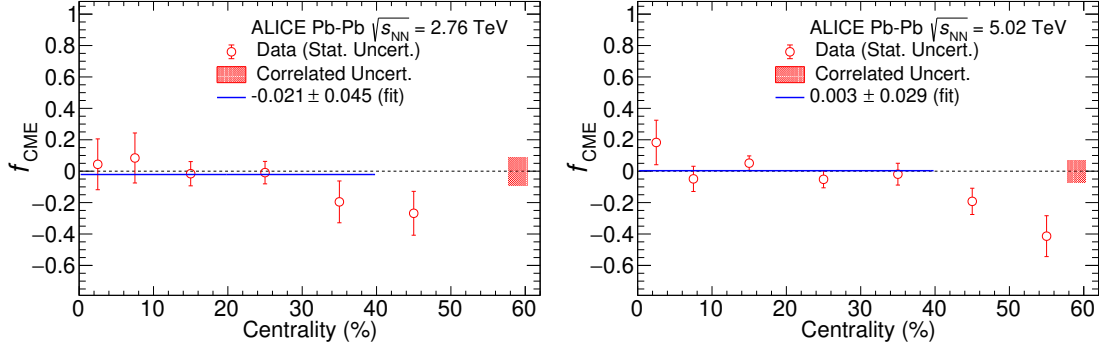
Figure 8. (Left panel) The CME fraction extracted in Pb-Pb collisions at $\sqrt{s_{\mathrm{NN}}} = 2.76\,\mathrm{TeV}$. (Right panel) The CME fraction extracted in Pb-Pb collisions at $\sqrt{s_{\mathrm{NN}}} = 5.02\,\mathrm{TeV}$. The systematic uncertainty is shown as hatched band at zero line around the centrality value of 60%. The solid blue lines correspond to fit with a constant function to the data points. See text for details.

the $\gamma_{1,-3}$ correlator ambiguous to extract the CME contribution at this stage. Therefore, in the following we only use $\gamma_{1,1}$ correlator to make quantitative measurement of CME. The values of v_2 and v_3 used to scale the charge-dependent differences of $\gamma_{1,1}$ and $\gamma_{1,2}$, are the ones measured by ALICE in Pb-Pb collisions reported in ref. [62] and ref. [58] for $\sqrt{s_{\mathrm{NN}}} = 2.76\,\mathrm{TeV}$ and $\sqrt{s_{\mathrm{NN}}} = 5.02\,\mathrm{TeV}$, respectively. The value of v_2 is estimated as the average of $v_2\{2\}$ and $v_2\{4\}$ to reduce the biases due to fluctuations assuming a Gaussian probability distribution [64]. Assuming $\kappa_2 \approx \kappa_3$ as supported by the model study, the value of $\Delta\gamma_{1,2} \times v_2/v_3$ was used according to eq. (3.7) as a proxy for the magnitude of the background contribution to the measurement of $\Delta\gamma_{1,1}$, denoted as $\Delta\gamma_{1,1}^{\mathrm{Bkg}}$, for both LHC energies. The CME fraction is then defined as

$$f_{\mathrm{CME}} = 1 - \frac{\Delta\gamma_{1,1}^{\mathrm{Bkg}}}{\Delta\gamma_{1,1}}, \tag{5.1}$$

where $\Delta\gamma_{1,1}$ is the measured value of the correlator presented on the left panel of figure 5. Figure 8 presents the centrality dependence of the CME fraction at $\sqrt{s_{\mathrm{NN}}} = 2.76\,\mathrm{TeV}$ (left plot) and $\sqrt{s_{\mathrm{NN}}} = 5.02\,\mathrm{TeV}$ (right plot). The systematic uncertainties on f_{CME} have been estimated from the same sources as mentioned in section 4. In addition, the contribution to the systematic uncertainty stemming from v_2 was also estimated using $v_2\{2\}$ in eq. (3.7) instead of the average of $v_2\{2\}$ and $v_2\{4\}$. All individual sources are then added in quadrature to get the total systematic uncertainty. We have excluded any systematic variation in the assumption of $\kappa_2 \approx \kappa_3$ for the reported values of f_{CME}.

The total, centrality-independent systematic uncertainty is indicated by the shaded box on the line at zero. It is seen that for both energies f_{CME} is compatible with zero up to centrality $\approx 40\%$. For more peripheral collisions, the value of f_{CME} is negative. There could be several possible reasons behind this observation. The event plane resolution starts to decline for peripheral events giving rise to fluctuations in the measured observables. The non-flow, the effect of which is negligible for $\Delta\gamma_{\mathrm{m,n}}$ but significant for v_{n}, can affect the measurement for peripheral events. There is another possibility that the ratio of the pro-

portionality constants, i.e, κ_2/κ_3 have a centrality dependence instead of being a constant. Therefore the observation of negative f_{CME} for peripheral events could be a convoluted effect of all these underlying phenomena. However, within the scope of this analysis, we have limited ourselves with constant behavior of κ_2/κ_3 as a function of centrality.

Finally, to estimate an upper limit on the contribution of the CME signal to the measurement of $\gamma_{1,1}$, the data points of f_{CME} are fitted with a constant function up to the 40% centrality interval. The fit yields values -0.021 ± 0.045 and 0.003 ± 0.029 in Pb-Pb collisions at $\sqrt{s_{\mathrm{NN}}} = 2.76$ and $5.02\,\mathrm{TeV}$, respectively. These results are consistent with zero CME fraction and correspond to upper limits on f_{CME} of 15–18% (20–24%) at 95% (99.7%) confidence level for the 0–40% centrality interval. The latter values are estimated assuming Gaussian distributed uncertainties and taking into account that the CME fraction has a lower bound of 0 (see figure 8).

6   Summary

In this article, we reported charge-dependent results for various two-particle correlators as well as two-particle correlations relative to different order symmetry planes. These measurements are extracted from the analysis of Pb-Pb collisions recorded by ALICE at $\sqrt{s_{\mathrm{NN}}} = 2.76$ and $5.02\,\mathrm{TeV}$. These correlators exhibit different sensitivity to the signal induced by the CME and to background effects, dominated by local charge conservations coupled to anisotropic flow.

All two-particle correlations of the form δ_{m} for m = 1, 2, 3 and 4 are dominated by background effects and exhibit a significant centrality dependence. Among them, only δ_1 exhibits a notable charge-dependent difference, which does not change significantly as a function of Δp_{T}, but increases with increasing $\overline{p_{\mathrm{T}}}$ and decreases with increasing $\Delta\eta$ of the pair. For higher harmonics, on the other hand, the charge-dependent differences become progressively smaller and are compatible with zero for δ_3 and δ_4.

The CME sensitive two-particle correlations relative to the second order symmetry plane, $\gamma_{1,1}$ and $\gamma_{1,-3}$, exhibit a significant charge-dependent difference, which increases towards peripheral centrality intervals. Results on particle correlations relative to the third order symmetry plane, expressed by $\gamma_{1,2}$, that probe background effects associated with local charge conservation modulated by triangular flow (v_3), also show a significant charge-dependent difference, which increases for more peripheral events. Finally, correlations between two particles relative to the fourth order symmetry plane, that also have the potential to probe mainly background effects, show no significant difference for pairs with same and opposite electric charges, however they are suffering from large statistical and systematic uncertainties.

A blast wave parametrisation that incorporates local charge conservation tuned to reproduce the components of the background, is not able to fully describe the magnitude of the charge-dependent differences of the CME-sensitive correlator $\gamma_{1,1}$. Finally, the results of correlations relative to Ψ_3 and Ψ_4 that probe mainly, if not solely, the contribution of the background clearly show that these background effects are the dominating factor to the measurements of $\gamma_{1,1}$.

Acknowledgments

References

[1] E.V. Shuryak, *Theory and phenomenology of the QCD vacuum*, *Phys. Rept.* **115** (1984) 151 [INSPIRE].

[2] J. Cleymans, R.V. Gavai and E. Suhonen, *Quarks and gluons at high temperatures and densities*, *Phys. Rept.* **130** (1986) 217 [INSPIRE].

[3] S.A. Bass, M. Gyulassy, H. Stoecker and W. Greiner, *Signatures of quark gluon plasma formation in high-energy heavy ion collisions: a critical review*, *J. Phys. G* **25** (1999) R1 [hep-ph/9810281] [INSPIRE].

[4] S. Borsányi et al., *The QCD equation of state with dynamical quarks*, *JHEP* **11** (2010) 077 [arXiv:1007.2580] [INSPIRE].

[5] T. Bhattacharya et al., *QCD phase transition with chiral quarks and physical quark masses*, *Phys. Rev. Lett.* **113** (2014) 082001 [arXiv:1402.5175] [INSPIRE].

[6] T.D. Lee, *A theory of spontaneous T violation*, *Phys. Rev. D* **8** (1973) 1226 [INSPIRE].

[7] T.D. Lee and G.C. Wick, *Vacuum stability and vacuum excitation in a spin 0 field theory*, *Phys. Rev. D* **9** (1974) 2291 [INSPIRE].

[8] A. Bzdak and V. Skokov, *Event-by-event fluctuations of magnetic and electric fields in heavy ion collisions*, *Phys. Lett. B* **710** (2012) 171 [arXiv:1111.1949] [INSPIRE].

[9] P.D. Morley and I.A. Schmidt, *Strong P, CP, T violations in heavy ion collisions*, *Z. Phys. C* **26** (1985) 627 [INSPIRE].

[10] D. Kharzeev, R.D. Pisarski and M.H.G. Tytgat, *Possibility of spontaneous parity violation in hot QCD*, *Phys. Rev. Lett.* **81** (1998) 512 [hep-ph/9804221] [INSPIRE].

[11] D. Kharzeev and R.D. Pisarski, *Pionic measures of parity and CP-violation in high-energy nuclear collisions*, *Phys. Rev. D* **61** (2000) 111901 [hep-ph/9906401] [INSPIRE].

[12] D.E. Kharzeev, *The Chiral Magnetic Effect and anomaly-induced transport*, *Prog. Part. Nucl. Phys.* **75** (2014) 133 [arXiv:1312.3348] [INSPIRE].

[13] D.E. Kharzeev, *Topology, magnetic field, and strongly interacting matter*, *Ann. Rev. Nucl. Part. Sci.* **65** (2015) 193 [arXiv:1501.01336] [INSPIRE].

[14] D. Kharzeev and A. Zhitnitsky, *Charge separation induced by P-odd bubbles in QCD matter*, *Nucl. Phys. A* **797** (2007) 67 [arXiv:0706.1026] [INSPIRE].

[15] K. Fukushima, D.E. Kharzeev and H.J. Warringa, *The chiral magnetic effect*, *Phys. Rev. D* **78** (2008) 074033 [arXiv:0808.3382] [INSPIRE].

[16] D.E. Kharzeev, L.D. McLerran and H.J. Warringa, *The effects of topological charge change in heavy ion collisions: 'Event by event P and CP-violation'*, *Nucl. Phys. A* **803** (2008) 227 [arXiv:0711.0950] [INSPIRE].

[17] Q. Li et al., *Observation of the chiral magnetic effect in $ZrTe_5$*, *Nature Phys.* **12** (2016) 550 [arXiv:1412.6543] [INSPIRE].

[18] S. Voloshin and Y. Zhang, *Flow study in relativistic nuclear collisions by Fourier expansion of Azimuthal particle distributions*, *Z. Phys. C* **70** (1996) 665 [hep-ph/9407282] [INSPIRE].

[19] PHOBOS collaboration, *System size, energy and pseudorapidity dependence of directed and elliptic flow at RHIC*, *Nucl. Phys. A* **774** (2006) 523 [nucl-ex/0510031] [INSPIRE].

[20] R.S. Bhalerao and J.-Y. Ollitrault, *Eccentricity fluctuations and elliptic flow at RHIC*, *Phys. Lett. B* **641** (2006) 260 [nucl-th/0607009] [INSPIRE].

[21] PHOBOS collaboration, *Importance of correlations and fluctuations on the initial source eccentricity in high-energy nucleus-nucleus collisions*, *Phys. Rev. C* **77** (2008) 014906 [arXiv:0711.3724] [INSPIRE].

[22] B. Alver and G. Roland, *Collision geometry fluctuations and triangular flow in heavy-ion collisions*, *Phys. Rev. C* **81** (2010) 054905 [*Erratum ibid.* **82** (2010) 039903] [arXiv:1003.0194] [INSPIRE].

[23] B.H. Alver, C. Gombeaud, M. Luzum and J.-Y. Ollitrault, *Triangular flow in hydrodynamics and transport theory*, *Phys. Rev. C* **82** (2010) 034913 [arXiv:1007.5469] [INSPIRE].

[24] S.A. Voloshin, *Parity violation in hot QCD: How to detect it*, *Phys. Rev. C* **70** (2004) 057901 [hep-ph/0406311] [INSPIRE].

[25] ALICE collaboration, *Charge separation relative to the reaction plane in Pb-Pb collisions at $\sqrt{s_{NN}} = 2.76$ TeV*, *Phys. Rev. Lett.* **110** (2013) 012301 [arXiv:1207.0900] [INSPIRE].

[26] STAR collaboration, *Azimuthal charged-particle correlations and possible local strong parity violation*, *Phys. Rev. Lett.* **103** (2009) 251601 [arXiv:0909.1739] [INSPIRE].

[27] STAR collaboration, *Observation of charge-dependent azimuthal correlations and possible local strong parity violation in heavy ion collisions*, *Phys. Rev. C* **81** (2010) 054908 [arXiv:0909.1717] [INSPIRE].

[28] STAR collaboration, *Measurement of charge multiplicity asymmetry correlations in high-energy nucleus-nucleus collisions at $\sqrt{s_{NN}} = 200$ GeV*, *Phys. Rev. C* **89** (2014) 044908 [arXiv:1303.0901] [INSPIRE].

[29] STAR collaboration, *Fluctuations of charge separation perpendicular to the event plane and local parity violation in $\sqrt{s_{NN}} = 200$ GeV Au+Au collisions at the BNL Relativistic Heavy Ion Collider*, *Phys. Rev. C* **88** (2013) 064911 [arXiv:1302.3802] [INSPIRE].

[30] STAR collaboration, *Beam-energy dependence of charge separation along the magnetic field in Au+Au collisions at RHIC*, *Phys. Rev. Lett.* **113** (2014) 052302 [arXiv:1404.1433] [INSPIRE].

[31] S. Schlichting and S. Pratt, *Charge conservation at energies available at the BNL Relativistic Heavy Ion Collider and contributions to local parity violation observables*, *Phys. Rev. C* **83** (2011) 014913 [arXiv:1009.4283] [INSPIRE].

[32] S. Pratt, S. Schlichting and S. Gavin, *Effects of momentum conservation and flow on angular correlations at RHIC*, *Phys. Rev. C* **84** (2011) 024909 [arXiv:1011.6053] [INSPIRE].

[33] ALICE collaboration, *Constraining the magnitude of the Chiral Magnetic Effect with event shape engineering in Pb-Pb collisions at $\sqrt{s_{NN}} = 2.76$ TeV*, *Phys. Lett. B* **777** (2018) 151 [arXiv:1709.04723] [INSPIRE].

[34] J. Schukraft, A. Timmins and S.A. Voloshin, *Ultra-relativistic nuclear collisions: event shape engineering*, *Phys. Lett. B* **719** (2013) 394 [arXiv:1208.4563] [INSPIRE].

[35] CMS collaboration, *Observation of charge-dependent azimuthal correlations in p-Pb collisions and its implication for the search for the chiral magnetic effect*, *Phys. Rev. Lett.* **118** (2017) 122301 [arXiv:1610.00263] [INSPIRE].

[36] STAR collaboration, *Charge-dependent pair correlations relative to a third particle in p+Au and d+Au collisions at RHIC*, *Phys. Lett. B* **798** (2019) 134975 [arXiv:1906.03373] [INSPIRE].

[37] CMS collaboration, *Constraints on the chiral magnetic effect using charge-dependent azimuthal correlations in p-Pb and Pb-Pb collisions at the CERN Large Hadron Collider*, *Phys. Rev. C* **97** (2018) 044912 [arXiv:1708.01602] [INSPIRE].

[38] ATLAS collaboration, *Measurement of event-plane correlations in $\sqrt{s_{NN}} = 2.76$ TeV lead-lead collisions with the ATLAS detector*, *Phys. Rev. C* **90** (2014) 024905 [arXiv:1403.0489] [INSPIRE].

[39] S.A. Voloshin, *Collective phenomena in ultra-relativistic nuclear collisions: anisotropic flow and more*, *Prog. Part. Nucl. Phys.* **67** (2012) 541 [arXiv:1111.7241] [INSPIRE].

[40] ALICE collaboration, *The ALICE experiment at the CERN LHC*, 2008 *JINST* **3** S08002 [INSPIRE].

[41] J. Alme et al., *The ALICE TPC, a large 3-dimensional tracking device with fast readout for ultra-high multiplicity events*, *Nucl. Instrum. Meth. A* **622** (2010) 316 [arXiv:1001.1950] [INSPIRE].

[42] ALICE collaboration, *Performance of the ALICE VZERO system*, 2013 *JINST* **8** P10016 [arXiv:1306.3130] [INSPIRE].

[43] ALICE collaboration, *Performance of the ALICE experiment at the CERN LHC*, *Int. J. Mod. Phys. A* **29** (2014) 1430044 [arXiv:1402.4476] [INSPIRE].

[44] ALICE collaboration, *Centrality determination of Pb-Pb collisions at $\sqrt{s_{NN}} = 2.76$ TeV with ALICE*, *Phys. Rev. C* **88** (2013) 044909 [arXiv:1301.4361] [INSPIRE].

[45] P. Billoir, *Track fitting with multiple scattering: a new method*, *Nucl. Instrum. Meth. A* **225** (1984) 352 [INSPIRE].

[46] P. Billoir, R. Fruhwirth and M. Regler, *Track element merging strategy and vertex fitting in complex modular detectors*, *Nucl. Instrum. Meth. A* **241** (1985) 115 [INSPIRE].

[47] U. Gursoy, D. Kharzeev, E. Marcus, K. Rajagopal and C. Shen, *Charge-dependent flow induced by magnetic and electric fields in heavy ion collisions*, *Phys. Rev. C* **98** (2018) 055201 [arXiv:1806.05288] [INSPIRE].

[48] A. Bzdak, V. Koch and J. Liao, *Charge-dependent correlations in relativistic heavy ion collisions and the chiral magnetic effect*, *Lect. Notes Phys.* **871** (2013) 503 [arXiv:1207.7327] [INSPIRE].

[49] F. Retiere and M.A. Lisa, *Observable implications of geometrical and dynamical aspects of freeze out in heavy ion collisions*, *Phys. Rev. C* **70** (2004) 044907 [nucl-th/0312024] [INSPIRE].

[50] B. Zhang, C.M. Ko, B.-A. Li and Z.-w. Lin, *A multiphase transport model for nuclear collisions at RHIC*, *Phys. Rev. C* **61** (2000) 067901 [nucl-th/9907017] [INSPIRE].

[51] Z.-w. Lin, S. Pal, C.M. Ko, B.-A. Li and B. Zhang, *Charged particle rapidity distributions at relativistic energies*, *Phys. Rev. C* **64** (2001) 011902 [nucl-th/0011059] [INSPIRE].

[52] Z.-W. Lin, C.M. Ko, B.-A. Li, B. Zhang and S. Pal, *A multi-phase transport model for relativistic heavy ion collisions*, *Phys. Rev. C* **72** (2005) 064901 [nucl-th/0411110] [INSPIRE].

[53] A.M. Poskanzer and S.A. Voloshin, *Methods for analyzing anisotropic flow in relativistic nuclear collisions*, *Phys. Rev. C* **58** (1998) 1671 [nucl-ex/9805001] [INSPIRE].

[54] S.A. Voloshin, A.M. Poskanzer and R. Snellings, *Collective phenomena in non-central nuclear collisions*, in *Relativistic heavy ion physics*, R. Stock ed., Landolt-Bornstein volume 23, Springer, Germany (2010) [arXiv:0809.2949] [INSPIRE].

[55] R. Barlow, *Systematic errors: Facts and fictions*, in the proceedings of the *Conference on Advanced Statistical Techniques in Particle Physics*, March 18–22, Durham U.K. (2002) [hep-ex/0207026] [INSPIRE].

[56] ALICE collaboration, *Charge correlations using the balance function in Pb-Pb collisions at $\sqrt{s_{NN}} = 2.76$ TeV*, *Phys. Lett. B* **723** (2013) 267 [arXiv:1301.3756] [INSPIRE].

[57] ALICE collaboration, *Multiplicity and transverse momentum evolution of charge-dependent correlations in pp, p-Pb, and Pb-Pb collisions at the LHC*, *Eur. Phys. J. C* **76** (2016) 86 [arXiv:1509.07255] [INSPIRE].

[58] ALICE collaboration, *Energy dependence and fluctuations of anisotropic flow in Pb-Pb collisions at $\sqrt{s_{NN}} = 5.02$ and 2.76 TeV*, *JHEP* **07** (2018) 103 [arXiv:1804.02944] [INSPIRE].

[59] ALICE collaboration, *Production of charged pions, kaons, and (anti-)protons in Pb-Pb and inelastic pp collisions at $\sqrt{s_{NN}} = 5.02$ TeV*, *Phys. Rev. C* **101** (2020) 044907 [arXiv:1910.07678] [INSPIRE].

[60] ALICE collaboration, *Anisotropic flow of identified particles in Pb-Pb collisions at $\sqrt{s_{NN}} = 5.02$ TeV*, *JHEP* **09** (2018) 006 [arXiv:1805.04390] [INSPIRE].

[61] B. Zhang, *ZPC 1.0.1: a parton cascade for ultrarelativistic heavy ion collisions*, *Comput. Phys. Commun.* **109** (1998) 193 [`nucl-th/9709009`] [ɪɴSPIRE].

[62] ALICE collaboration, *Elliptic flow of charged particles in Pb-Pb collisions at 2.76 TeV*, *Phys. Rev. Lett.* **105** (2010) 252302 [`arXiv:1011.3914`] [ɪɴSPIRE].

[63] S. Choudhury, G. Wang, W. He, Y. Hu and H.Z. Huang, *Background evaluations for the chiral magnetic effect with normalized correlators using a multiphase transport model*, *Eur. Phys. J. C* **80** (2020) 383 [`arXiv:1909.04083`] [ɪɴSPIRE].

[64] S.A. Voloshin, A.M. Poskanzer, A. Tang and G. Wang, *Elliptic flow in the Gaussian model of eccentricity fluctuations*, *Phys. Lett. B* **659** (2008) 537 [`arXiv:0708.0800`] [ɪɴSPIRE].

The ALICE collaboration

S. Acharya[141], D. Adamová[95], A. Adler[74], J. Adolfsson[81], M.M. Aggarwal[100], G. Aglieri Rinella[34],
M. Agnello[30], N. Agrawal[10,54], Z. Ahammed[141], S. Ahmad[16], S.U. Ahn[76], Z. Akbar[51],
A. Akindinov[92], M. Al-Turany[107], S.N. Alam[40,141], D.S.D. Albuquerque[122], D. Aleksandrov[88],
B. Alessandro[59], H.M. Alfanda[6], R. Alfaro Molina[71], B. Ali[16], Y. Ali[14], A. Alici[10,26,54],
A. Alkin[2,34], J. Alme[21], T. Alt[68], L. Altenkamper[21], I. Altsybeev[113], M.N. Anaam[6], C. Andrei[48],
D. Andreou[34], A. Andronic[144], M. Angeletti[34], V. Anguelov[104], C. Anson[15], T. Antičić[108],
F. Antinori[57], P. Antonioli[54], N. Apadula[80], L. Aphecetche[115], H. Appelshäuser[68], S. Arcelli[26],
R. Arnaldi[59], M. Arratia[80], I.C. Arsene[20], M. Arslandok[104], A. Augustinus[34], R. Averbeck[107],
S. Aziz[78], M.D. Azmi[16], A. Badalà[56], Y.W. Baek[41], S. Bagnasco[59], X. Bai[107], R. Bailhache[68],
R. Bala[101], A. Balbino[30], A. Baldisseri[137], M. Ball[43], S. Balouza[105], D. Banerjee[3], R. Barbera[27],
L. Barioglio[25], G.G. Barnaföldi[145], L.S. Barnby[94], V. Barret[134], P. Bartalini[6], C. Bartels[127],
K. Barth[34], E. Bartsch[68], F. Baruffaldi[28], N. Bastid[134], S. Basu[143], G. Batigne[115], B. Batyunya[75],
D. Bauri[49], J.L. Bazo Alba[112], I.G. Bearden[89], C. Beattie[146], C. Bedda[63], N.K. Behera[61],
I. Belikov[136], A.D.C. Bell Hechavarria[144], F. Bellini[34], R. Bellwied[125], V. Belyaev[93],
G. Bencedi[145], S. Beole[25], A. Bercuci[48], Y. Berdnikov[98], A. Berdnikova[104], D. Berenyi[145],
R.A. Bertens[130], D. Berzano[59], M.G. Besoiu[67], L. Betev[34], A. Bhasin[101], I.R. Bhat[101],
M.A. Bhat[3], H. Bhatt[49], B. Bhattacharjee[42], A. Bianchi[25], L. Bianchi[25], N. Bianchi[52],
J. Bielčík[37], J. Bielčíková[95], A. Bilandzic[105], G. Biro[145], R. Biswas[3], S. Biswas[3], J.T. Blair[119],
D. Blau[88], C. Blume[68], G. Boca[139], F. Bock[96], A. Bogdanov[93], S. Boi[23], J. Bok[61], L. Boldizsár[145],
A. Bolozdynya[93], M. Bombara[38], G. Bonomi[140], H. Borel[137], A. Borissov[93], H. Bossi[146],
E. Botta[25], L. Bratrud[68], P. Braun-Munzinger[107], M. Bregant[121], M. Broz[37], E. Bruna[59],
G.E. Bruno[106], M.D. Buckland[127], D. Budnikov[109], H. Buesching[68], S. Bufalino[30], O. Bugnon[115],
P. Buhler[114], P. Buncic[34], Z. Buthelezi[72,131], J.B. Butt[14], S.A. Bysiak[118], D. Caffarri[90],
A. Caliva[107], E. Calvo Villar[112], R.S. Camacho[45], P. Camerini[24], A.A. Capon[114],
F. Carnesecchi[26], R. Caron[137], J. Castillo Castellanos[137], A.J. Castro[130], E.A.R. Casula[55],
F. Catalano[30], C. Ceballos Sanchez[53], P. Chakraborty[49], S. Chandra[141], W. Chang[6],
S. Chapeland[34], M. Chartier[127], S. Chattopadhyay[141], S. Chattopadhyay[110], A. Chauvin[23],
C. Cheshkov[135], B. Cheynis[135], V. Chibante Barroso[34], D.D. Chinellato[122], S. Cho[61],
P. Chochula[34], T. Chowdhury[134], P. Christakoglou[90], C.H. Christensen[89], P. Christiansen[81],
T. Chujo[133], C. Cicalo[55], L. Cifarelli[10,26], F. Cindolo[54], G. Clai[54, ii], J. Cleymans[124],
F. Colamaria[53], D. Colella[53], A. Collu[80], M. Colocci[26], M. Concas[59, iii], G. Conesa Balbastre[79],
Z. Conesa del Valle[78], G. Contin[24,60], J.G. Contreras[37], T.M. Cormier[96], Y. Corrales Morales[25],
P. Cortese[31], M.R. Cosentino[123], F. Costa[34], S. Costanza[139], P. Crochet[134], E. Cuautle[69], P. Cui[6],
L. Cunqueiro[96], D. Dabrowski[142], T. Dahms[105], A. Dainese[57], F.P.A. Damas[115,137],
M.C. Danisch[104], A. Danu[67], D. Das[110], I. Das[110], P. Das[86], P. Das[3], S. Das[3], A. Dash[86],
S. Dash[49], S. De[86], A. De Caro[29], G. de Cataldo[53], J. de Cuveland[39], A. De Falco[23], D. De
Gruttola[10], N. De Marco[59], S. De Pasquale[29], S. Deb[50], H.F. Degenhardt[121], K.R. Deja[142],
A. Deloff[85], S. Delsanto[25,131], W. Deng[6], P. Dhankher[49], D. Di Bari[33], A. Di Mauro[34],
R.A. Diaz[8], T. Dietel[124], P. Dillenseger[68], Y. Ding[6], R. Divià[34], D.U. Dixit[19], Ø. Djuvsland[21],
U. Dmitrieva[62], A. Dobrin[67], B. Dönigus[68], O. Dordic[20], A.K. Dubey[141], A. Dubla[90,107],
S. Dudi[100], M. Dukhishyam[86], P. Dupieux[134], R.J. Ehlers[96,146], V.N. Eikeland[21], D. Elia[53],
B. Erazmus[115], F. Erhardt[99], A. Erokhin[113], M.R. Ersdal[21], B. Espagnon[78], G. Eulisse[34],
D. Evans[111], S. Evdokimov[91], L. Fabbietti[105], M. Faggin[28], J. Faivre[79], F. Fan[6], A. Fantoni[52],
M. Fasel[96], P. Fecchio[30], A. Feliciello[59], G. Feofilov[113], A. Fernández Téllez[45], A. Ferrero[137],
A. Ferretti[25], A. Festanti[34], V.J.G. Feuillard[104], J. Figiel[118], S. Filchagin[109], D. Finogeev[62],
F.M. Fionda[21], G. Fiorenza[53], F. Flor[125], A.N. Flores[119], S. Foertsch[72], P. Foka[107], S. Fokin[88],

E. Fragiacomo[60], U. Frankenfeld[107], U. Fuchs[34], C. Furget[79], A. Furs[62], M. Fusco Girard[29],
J.J. Gaardhøje[89], M. Gagliardi[25], A.M. Gago[112], A. Gal[136], C.D. Galvan[120], P. Ganoti[84],
C. Garabatos[107], J.R.A. Garcia[45], E. Garcia-Solis[11], K. Garg[115], C. Gargiulo[34], A. Garibli[87],
K. Garner[144], P. Gasik[105,107], E.F. Gauger[119], M.B. Gay Ducati[70], M. Germain[115], J. Ghosh[110],
P. Ghosh[141], S.K. Ghosh[3], M. Giacalone[26], P. Gianotti[52], P. Giubellino[59,107], P. Giubilato[28],
P. Glässel[104], A. Gomez Ramirez[74], V. Gonzalez[107,143], L.H. González-Trueba[71], S. Gorbunov[39],
L. Görlich[118], A. Goswami[49], S. Gotovac[35], V. Grabski[71], L.K. Graczykowski[142], K.L. Graham[111],
L. Greiner[80], A. Grelli[63], C. Grigoras[34], V. Grigoriev[93], A. Grigoryan[1], S. Grigoryan[75],
O.S. Groettvik[21], F. Grosa[30,59], J.F. Grosse-Oetringhaus[34], R. Grosso[107], R. Guernane[79],
M. Guittiere[115], K. Gulbrandsen[89], T. Gunji[132], A. Gupta[101], R. Gupta[101], I.B. Guzman[45],
R. Haake[146], M.K. Habib[107], C. Hadjidakis[78], H. Hamagaki[82], G. Hamar[145], M. Hamid[6],
R. Hannigan[119], M.R. Haque[63,86], A. Harlenderova[107], J.W. Harris[146], A. Harton[11],
J.A. Hasenbichler[34], H. Hassan[96], Q.U. Hassan[14], D. Hatzifotiadou[10,54], P. Hauer[43],
L.B. Havener[146], S. Hayashi[132], S.T. Heckel[105], E. Hellbär[68], H. Helstrup[36], A. Herghelegiu[48],
T. Herman[37], E.G. Hernandez[45], G. Herrera Corral[9], F. Herrmann[144], K.F. Hetland[36],
H. Hillemanns[34], C. Hills[127], B. Hippolyte[136], B. Hohlweger[105], J. Honermann[144], D. Horak[37],
A. Hornung[68], S. Hornung[107], R. Hosokawa[15], P. Hristov[34], C. Huang[78], C. Hughes[130], P. Huhn[68],
T.J. Humanic[97], H. Hushnud[110], L.A. Husova[144], N. Hussain[42], S.A. Hussain[14], D. Hutter[39],
J.P. Iddon[34,127], R. Ilkaev[109], H. Ilyas[14], M. Inaba[133], G.M. Innocenti[34], M. Ippolitov[88],
A. Isakov[95], M.S. Islam[110], M. Ivanov[107], V. Ivanov[98], V. Izucheev[91], B. Jacak[80], N. Jacazio[34,54],
P.M. Jacobs[80], S. Jadlovska[117], J. Jadlovsky[117], S. Jaelani[63], C. Jahnke[121], M.J. Jakubowska[142],
M.A. Janik[142], T. Janson[74], M. Jercic[99], O. Jevons[111], M. Jin[125], F. Jonas[96,144], P.G. Jones[111],
J. Jung[68], M. Jung[68], A. Jusko[111], P. Kalinak[64], A. Kalweit[34], V. Kaplin[93], S. Kar[6], A. Karasu
Uysal[77], O. Karavichev[62], T. Karavicheva[62], P. Karczmarczyk[34], E. Karpechev[62], A. Kazantsev[88],
U. Kebschull[74], R. Keidel[47], M. Keil[34], B. Ketzer[43], Z. Khabanova[90], A.M. Khan[6], S. Khan[16],
S.A. Khan[141], A. Khanzadeev[98], Y. Kharlov[91], A. Khatun[16], A. Khuntia[118], B. Kileng[36],
B. Kim[61], B. Kim[133], D. Kim[147], D.J. Kim[126], E.J. Kim[73], H. Kim[17], J. Kim[147], J.S. Kim[41],
J. Kim[104], J. Kim[147], J. Kim[73], M. Kim[104], S. Kim[18], T. Kim[147], T. Kim[147], S. Kirsch[68],
I. Kisel[39], S. Kiselev[92], A. Kisiel[142], J.L. Klay[5], C. Klein[68], J. Klein[34,59], S. Klein[80],
C. Klein-Bösing[144], M. Kleiner[68], A. Kluge[34], M.L. Knichel[34], A.G. Knospe[125], C. Kobdaj[116],
M.K. Köhler[104], T. Kollegger[107], A. Kondratyev[75], N. Kondratyeva[93], E. Kondratyuk[91],
J. Konig[68], S.A. Konigstorfer[105], P.J. Konopka[34], G. Kornakov[142], L. Koska[117], O. Kovalenko[85],
V. Kovalenko[113], M. Kowalski[118], I. Králik[64], A. Kravčáková[38], L. Kreis[107], M. Krivda[64,111],
F. Krizek[95], K. Krizkova Gajdosova[37], M. Krüger[68], E. Kryshen[98], M. Krzewicki[39],
A.M. Kubera[97], V. Kučera[34,61], C. Kuhn[136], P.G. Kuijer[90], L. Kumar[100], S. Kundu[86],
P. Kurashvili[85], A. Kurepin[62], A.B. Kurepin[62], A. Kuryakin[109], S. Kushpil[95], J. Kvapil[111],
M.J. Kweon[61], J.Y. Kwon[61], Y. Kwon[147], S.L. La Pointe[39], P. La Rocca[27], Y.S. Lai[80],
M. Lamanna[34], R. Langoy[129], K. Lapidus[34], A. Lardeux[20], P. Larionov[52], E. Laudi[34],
R. Lavicka[37], T. Lazareva[113], R. Lea[24], L. Leardini[104], J. Lee[133], S. Lee[147], F. Lehas[90],
S. Lehner[114], J. Lehrbach[39], R.C. Lemmon[94], I. León Monzón[120], E.D. Lesser[19], M. Lettrich[34],
P. Lévai[145], X. Li[12], X.L. Li[6], J. Lien[129], R. Lietava[111], B. Lim[17], V. Lindenstruth[39], A. Lindner[48],
C. Lippmann[107], M.A. Lisa[97], A. Liu[19], J. Liu[127], S. Liu[97], W.J. Llope[143], I.M. Lofnes[21],
V. Loginov[93], C. Loizides[96], P. Loncar[35], J.A. Lopez[104], X. Lopez[134], E. López Torres[8],
J.R. Luhder[144], M. Lunardon[28], G. Luparello[60], Y.G. Ma[40], A. Maevskaya[62], M. Mager[34],
S.M. Mahmood[20], T. Mahmoud[43], A. Maire[136], R.D. Majka[146, i], M. Malaev[98], Q.W. Malik[20],
L. Malinina[75, iv], D. Mal'Kevich[92], P. Malzacher[107], G. Mandaglio[32,56], V. Manko[88], F. Manso[134],
V. Manzari[53], Y. Mao[6], M. Marchisone[135], J. Mareš[66], G.V. Margagliotti[24], A. Margotti[54],
J. Margutti[63], A. Marín[107], C. Markert[119], M. Marquard[68], C.D. Martin[24], N.A. Martin[104],

P. Martinengo[34], J.L. Martinez[125], M.I. Martínez[45], G. Martínez García[115], S. Masciocchi[107], M. Masera[25], A. Masoni[55], L. Massacrier[78], E. Masson[115], A. Mastroserio[53,138], A.M. Mathis[105], O. Matonoha[81], P.F.T. Matuoka[121], A. Matyja[118], C. Mayer[118], F. Mazzaschi[25], M. Mazzilli[53], M.A. Mazzoni[58], A.F. Mechler[68], F. Meddi[22], Y. Melikyan[62,93], A. Menchaca-Rocha[71], C. Mengke[6], E. Meninno[29,114], M. Meres[13], S. Mhlanga[124], Y. Miake[133], L. Micheletti[25], L.C. Migliorin[135], D.L. Mihaylov[105], K. Mikhaylov[75,92], A.N. Mishra[69], D. Miśkowiec[107], A. Modak[3], N. Mohammadi[34], A.P. Mohanty[63], B. Mohanty[86], M. Mohisin Khan[16, v], Z. Moravcova[89], C. Mordasini[105], D.A. Moreira De Godoy[144], L.A.P. Moreno[45], I. Morozov[62], A. Morsch[34], T. Mrnjavac[34], V. Muccifora[52], E. Mudnic[35], D. Mühlheim[144], S. Muhuri[141], J.D. Mulligan[80], M.G. Munhoz[121], R.H. Munzer[68], H. Murakami[132], S. Murray[124], L. Musa[34], J. Musinsky[64], C.J. Myers[125], J.W. Myrcha[142], B. Naik[49], R. Nair[85], B.K. Nandi[49], R. Nania[10,54], E. Nappi[53], M.U. Naru[14], A.F. Nassirpour[81], C. Nattrass[130], R. Nayak[49], T.K. Nayak[86], S. Nazarenko[109], A. Neagu[20], R.A. Negrao De Oliveira[68], L. Nellen[69], S.V. Nesbo[36], G. Neskovic[39], D. Nesterov[113], L.T. Neumann[142], B.S. Nielsen[89], S. Nikolaev[88], S. Nikulin[88], V. Nikulin[98], F. Noferini[10,54], P. Nomokonov[75], J. Norman[79,127], N. Novitzky[133], P. Nowakowski[142], A. Nyanin[88], J. Nystrand[21], M. Ogino[82], A. Ohlson[81,104], J. Oleniacz[142], A.C. Oliveira Da Silva[130], M.H. Oliver[146], C. Oppedisano[59], A. Ortiz Velasquez[69], A. Oskarsson[81], J. Otwinowski[118], K. Oyama[82], Y. Pachmayer[104], V. Pacik[89], D. Pagano[140], G. Paić[69], J. Pan[143], S. Panebianco[137], P. Pareek[50,141], J. Park[61], J.E. Parkkila[126], S. Parmar[100], S.P. Pathak[125], B. Paul[23], J. Pazzini[140], H. Pei[6], T. Peitzmann[63], X. Peng[6], L.G. Pereira[70], H. Pereira Da Costa[137], D. Peresunko[88], G.M. Perez[8], Y. Pestov[4], V. Petráček[37], M. Petrovici[48], R.P. Pezzi[70], S. Piano[60], M. Pikna[13], P. Pillot[115], O. Pinazza[34,54], L. Pinsky[125], C. Pinto[27], S. Pisano[10,52], D. Pistone[56], M. Płoskoń[80], M. Planinic[99], F. Pliquett[68], M.G. Poghosyan[96], B. Polichtchouk[91], N. Poljak[99], A. Pop[48], S. Porteboeuf-Houssais[134], V. Pozdniakov[75], S.K. Prasad[3], R. Preghenella[54], F. Prino[59], C.A. Pruneau[143], I. Pshenichnov[62], M. Puccio[34], J. Putschke[143], S. Qiu[90], L. Quaglia[25], R.E. Quishpe[125], S. Ragoni[111], S. Raha[3], S. Rajput[101], J. Rak[126], A. Rakotozafindrabe[137], L. Ramello[31], F. Rami[136], S.A.R. Ramirez[45], R. Raniwala[102], S. Raniwala[102], S.S. Räsänen[44], R. Rath[50], V. Ratza[43], I. Ravasenga[90], K.F. Read[96,130], A.R. Redelbach[39], K. Redlich[85, vi], A. Rehman[21], P. Reichelt[68], F. Reidt[34], X. Ren[6], R. Renfordt[68], Z. Rescakova[38], K. Reygers[104], V. Riabov[98], T. Richert[81,89], M. Richter[20], P. Riedler[34], W. Riegler[34], F. Riggi[27], C. Ristea[67], S.P. Rode[50], M. Rodríguez Cahuantzi[45], K. Røed[20], R. Rogalev[91], E. Rogochaya[75], D. Rohr[34], D. Röhrich[21], P.F. Rojas[45], P.S. Rokita[142], F. Ronchetti[52], A. Rosano[56], E.D. Rosas[69], K. Roslon[142], A. Rossi[28,57], A. Rotondi[139], A. Roy[50], P. Roy[110], O.V. Rueda[81], R. Rui[24], B. Rumyantsev[75], A. Rustamov[87], E. Ryabinkin[88], Y. Ryabov[98], A. Rybicki[118], H. Rytkonen[126], O.A.M. Saarimaki[44], S. Sadhu[141], S. Sadovsky[91], K. Šafařík[37], S.K. Saha[141], B. Sahoo[49], P. Sahoo[49], R. Sahoo[50], S. Sahoo[65], P.K. Sahu[65], J. Saini[141], S. Sakai[133], S. Sambyal[101], V. Samsonov[93,98], D. Sarkar[143], N. Sarkar[141], P. Sarma[42], V.M. Sarti[105], M.H.P. Sas[63], E. Scapparone[54], J. Schambach[119], H.S. Scheid[68], C. Schiaua[48], R. Schicker[104], A. Schmah[104], C. Schmidt[107], H.R. Schmidt[103], M.O. Schmidt[104], M. Schmidt[103], N.V. Schmidt[68,96], A.R. Schmier[130], J. Schukraft[89], Y. Schutz[136], K. Schwarz[107], K. Schweda[107], G. Scioli[26], E. Scomparin[59], J.E. Seger[15], Y. Sekiguchi[132], D. Sekihata[132], I. Selyuzhenkov[93,107], S. Senyukov[136], D. Serebryakov[62], A. Sevcenco[67], A. Shabanov[62], A. Shabetai[115], R. Shahoyan[34], W. Shaikh[110], A. Shangaraev[91], A. Sharma[100], A. Sharma[101], H. Sharma[118], M. Sharma[101], N. Sharma[100], S. Sharma[101], K. Shigaki[46], M. Shimomura[83], S. Shirinkin[92], Q. Shou[40], Y. Sibiriak[88], S. Siddhanta[55], T. Siemiarczuk[85], D. Silvermyr[81], G. Simatovic[90], G. Simonetti[34], B. Singh[105], R. Singh[86], R. Singh[101], R. Singh[50], V.K. Singh[141], V. Singhal[141], T. Sinha[110], B. Sitar[13], M. Sitta[31], T.B. Skaali[20], M. Slupecki[44], N. Smirnov[146], R.J.M. Snellings[63], C. Soncco[112], J. Song[125], A. Songmoolnak[116], F. Soramel[28], S. Sorensen[130], I. Sputowska[118],

J. Stachel[104], I. Stan[67], P.J. Steffanic[130], E. Stenlund[81], S.F. Stiefelmaier[104], D. Stocco[115], M.M. Storetvedt[36], L.D. Stritto[29], A.A.P. Suaide[121], T. Sugitate[46], C. Suire[78], M. Suleymanov[14], M. Suljic[34], R. Sultanov[92], M. Šumbera[95], V. Sumberia[101], S. Sumowidagdo[51], S. Swain[65], A. Szabo[13], I. Szarka[13], U. Tabassam[14], S.F. Taghavi[105], G. Taillepied[134], J. Takahashi[122], G.J. Tambave[21], S. Tang[6,134], M. Tarhini[115], M.G. Tarzila[48], A. Tauro[34], G. Tejeda Muñoz[45], A. Telesca[34], L. Terlizzi[25], C. Terrevoli[125], D. Thakur[50], S. Thakur[141], D. Thomas[119], F. Thoresen[89], R. Tieulent[135], A. Tikhonov[62], A.R. Timmins[125], A. Toia[68], N. Topilskaya[62], M. Toppi[52], F. Torales-Acosta[19], S.R. Torres[37], A. Trifiró[32,56], S. Tripathy[50,69], T. Tripathy[49], S. Trogolo[28], G. Trombetta[33], L. Tropp[38], V. Trubnikov[2], W.H. Trzaska[126], T.P. Trzcinski[142], B.A. Trzeciak[37,63], A. Tumkin[109], R. Turrisi[57], T.S. Tveter[20], K. Ullaland[21], E.N. Umaka[125], A. Uras[135], G.L. Usai[23], M. Vala[38], N. Valle[139], S. Vallero[59], N. van der Kolk[63], L.V.R. van Doremalen[63], M. van Leeuwen[63], P. Vande Vyvre[34], D. Varga[145], Z. Varga[145], M. Varga-Kofarago[145], A. Vargas[45], M. Vasileiou[84], A. Vasiliev[88], O. Vázquez Doce[105], V. Vechernin[113], E. Vercellin[25], S. Vergara Limón[45], L. Vermunt[63], R. Vernet[7], R. Vértesi[145], L. Vickovic[35], Z. Vilakazi[131], O. Villalobos Baillie[111], G. Vino[53], A. Vinogradov[88], T. Virgili[29], V. Vislavicius[89], A. Vodopyanov[75], B. Volkel[34], M.A. Völkl[103], K. Voloshin[92], S.A. Voloshin[143], G. Volpe[33], B. von Haller[34], I. Vorobyev[105], D. Voscek[117], J. Vrláková[38], B. Wagner[21], M. Weber[114], S.G. Weber[144], A. Wegrzynek[34], S.C. Wenzel[34], J.P. Wessels[144], J. Wiechula[68], J. Wikne[20], G. Wilk[85], J. Wilkinson[10,54], G.A. Willems[144], E. Willsher[111], B. Windelband[104], M. Winn[137], W.E. Witt[130], J.R. Wright[119], Y. Wu[128], R. Xu[6], S. Yalcin[77], Y. Yamaguchi[46], K. Yamakawa[46], S. Yang[21], S. Yano[137], Z. Yin[6], H. Yokoyama[63], I.-K. Yoo[17], J.H. Yoon[61], S. Yuan[21], A. Yuncu[104], V. Yurchenko[2], V. Zaccolo[24], A. Zaman[14], C. Zampolli[34], H.J.C. Zanoli[63], N. Zardoshti[34], A. Zarochentsev[113], P. Závada[66], N. Zaviyalov[109], H. Zbroszczyk[142], M. Zhalov[98], S. Zhang[40], X. Zhang[6], Z. Zhang[6], V. Zherebchevskii[113], D. Zhou[6], Y. Zhou[89], Z. Zhou[21], J. Zhu[6,107], Y. Zhu[6], A. Zichichi[10,26], G. Zinovjev[2], N. Zurlo[140]

[i]   Deceased
[ii]   Italian National Agency for New Technologies, Energy and Sustainable Economic Development (ENEA), Bologna, Italy
[iii] Dipartimento DET del Politecnico di Torino, Turin, Italy
[iv]   M.V. Lomonosov Moscow State University, D.V. Skobeltsyn Institute of Nuclear, Physics, Moscow, Russia
[v]   Department of Applied Physics, Aligarh Muslim University, Aligarh, India
[vi]   Institute of Theoretical Physics, University of Wroclaw, Poland

[1]   A.I. Alikhanyan National Science Laboratory (Yerevan Physics Institute) Foundation, Yerevan, Armenia
[2]   Bogolyubov Institute for Theoretical Physics, National Academy of Sciences of Ukraine, Kiev, Ukraine
[3]   Bose Institute, Department of Physics and Centre for Astroparticle Physics and Space Science (CAPSS), Kolkata, India
[4]   Budker Institute for Nuclear Physics, Novosibirsk, Russia
[5]   California Polytechnic State University, San Luis Obispo, California, United States
[6]   Central China Normal University, Wuhan, China
[7]   Centre de Calcul de l'IN2P3, Villeurbanne, Lyon, France
[8]   Centro de Aplicaciones Tecnológicas y Desarrollo Nuclear (CEADEN), Havana, Cuba
[9]   Centro de Investigación y de Estudios Avanzados (CINVESTAV), Mexico City and Mérida, Mexico
[10]   Centro Fermi - Museo Storico della Fisica e Centro Studi e Ricerche "Enrico Fermi', Rome, Italy
[11]   Chicago State University, Chicago, Illinois, United States

12 *China Institute of Atomic Energy, Beijing, China*
13 *Comenius University Bratislava, Faculty of Mathematics, Physics and Informatics, Bratislava, Slovakia*
14 *COMSATS University Islamabad, Islamabad, Pakistan*
15 *Creighton University, Omaha, Nebraska, United States*
16 *Department of Physics, Aligarh Muslim University, Aligarh, India*
17 *Department of Physics, Pusan National University, Pusan, Republic of Korea*
18 *Department of Physics, Sejong University, Seoul, Republic of Korea*
19 *Department of Physics, University of California, Berkeley, California, United States*
20 *Department of Physics, University of Oslo, Oslo, Norway*
21 *Department of Physics and Technology, University of Bergen, Bergen, Norway*
22 *Dipartimento di Fisica dell'Università 'La Sapienza' and Sezione INFN, Rome, Italy*
23 *Dipartimento di Fisica dell'Università and Sezione INFN, Cagliari, Italy*
24 *Dipartimento di Fisica dell'Università and Sezione INFN, Trieste, Italy*
25 *Dipartimento di Fisica dell'Università and Sezione INFN, Turin, Italy*
26 *Dipartimento di Fisica e Astronomia dell'Università and Sezione INFN, Bologna, Italy*
27 *Dipartimento di Fisica e Astronomia dell'Università and Sezione INFN, Catania, Italy*
28 *Dipartimento di Fisica e Astronomia dell'Università and Sezione INFN, Padova, Italy*
29 *Dipartimento di Fisica 'E.R. Caianiello' dell'Università and Gruppo Collegato INFN, Salerno, Italy*
30 *Dipartimento DISAT del Politecnico and Sezione INFN, Turin, Italy*
31 *Dipartimento di Scienze e Innovazione Tecnologica dell'Università del Piemonte Orientale and INFN Sezione di Torino, Alessandria, Italy*
32 *Dipartimento di Scienze MIFT, Università di Messina, Messina, Italy*
33 *Dipartimento Interateneo di Fisica 'M. Merlin' and Sezione INFN, Bari, Italy*
34 *European Organization for Nuclear Research (CERN), Geneva, Switzerland*
35 *Faculty of Electrical Engineering, Mechanical Engineering and Naval Architecture, University of Split, Split, Croatia*
36 *Faculty of Engineering and Science, Western Norway University of Applied Sciences, Bergen, Norway*
37 *Faculty of Nuclear Sciences and Physical Engineering, Czech Technical University in Prague, Prague, Czech Republic*
38 *Faculty of Science, P.J. Šafárik University, Košice, Slovakia*
39 *Frankfurt Institute for Advanced Studies, Johann Wolfgang Goethe-Universität Frankfurt, Frankfurt, Germany*
40 *Fudan University, Shanghai, China*
41 *Gangneung-Wonju National University, Gangneung, Republic of Korea*
42 *Gauhati University, Department of Physics, Guwahati, India*
43 *Helmholtz-Institut für Strahlen- und Kernphysik, Rheinische Friedrich-Wilhelms-Universität Bonn, Bonn, Germany*
44 *Helsinki Institute of Physics (HIP), Helsinki, Finland*
45 *High Energy Physics Group, Universidad Autónoma de Puebla, Puebla, Mexico*
46 *Hiroshima University, Hiroshima, Japan*
47 *Hochschule Worms, Zentrum für Technologietransfer und Telekommunikation (ZTT), Worms, Germany*
48 *Horia Hulubei National Institute of Physics and Nuclear Engineering, Bucharest, Romania*
49 *Indian Institute of Technology Bombay (IIT), Mumbai, India*
50 *Indian Institute of Technology Indore, Indore, India*
51 *Indonesian Institute of Sciences, Jakarta, Indonesia*
52 *INFN, Laboratori Nazionali di Frascati, Frascati, Italy*
53 *INFN, Sezione di Bari, Bari, Italy*
54 *INFN, Sezione di Bologna, Bologna, Italy*
55 *INFN, Sezione di Cagliari, Cagliari, Italy*

[56] INFN, Sezione di Catania, Catania, Italy

[57] INFN, Sezione di Padova, Padova, Italy

[58] INFN, Sezione di Roma, Rome, Italy

[59] INFN, Sezione di Torino, Turin, Italy

[60] INFN, Sezione di Trieste, Trieste, Italy

[61] Inha University, Incheon, Republic of Korea

[62] Institute for Nuclear Research, Academy of Sciences, Moscow, Russia

[63] Institute for Subatomic Physics, Utrecht University/Nikhef, Utrecht, Netherlands

[64] Institute of Experimental Physics, Slovak Academy of Sciences, Košice, Slovakia

[65] Institute of Physics, Homi Bhabha National Institute, Bhubaneswar, India

[66] Institute of Physics of the Czech Academy of Sciences, Prague, Czech Republic

[67] Institute of Space Science (ISS), Bucharest, Romania

[68] Institut für Kernphysik, Johann Wolfgang Goethe-Universität Frankfurt, Frankfurt, Germany

[69] Instituto de Ciencias Nucleares, Universidad Nacional Autónoma de México, Mexico City, Mexico

[70] Instituto de Física, Universidade Federal do Rio Grande do Sul (UFRGS), Porto Alegre, Brazil

[71] Instituto de Física, Universidad Nacional Autónoma de México, Mexico City, Mexico

[72] iThemba LABS, National Research Foundation, Somerset West, South Africa

[73] Jeonbuk National University, Jeonju, Republic of Korea

[74] Johann-Wolfgang-Goethe Universität Frankfurt Institut für Informatik, Fachbereich Informatik und Mathematik, Frankfurt, Germany

[75] Joint Institute for Nuclear Research (JINR), Dubna, Russia

[76] Korea Institute of Science and Technology Information, Daejeon, Republic of Korea

[77] KTO Karatay University, Konya, Turkey

[78] Laboratoire de Physique des 2 Infinis, Irène Joliot-Curie, Orsay, France

[79] Laboratoire de Physique Subatomique et de Cosmologie, Université Grenoble-Alpes, CNRS-IN2P3, Grenoble, France

[80] Lawrence Berkeley National Laboratory, Berkeley, California, United States

[81] Lund University Department of Physics, Division of Particle Physics, Lund, Sweden

[82] Nagasaki Institute of Applied Science, Nagasaki, Japan

[83] Nara Women's University (NWU), Nara, Japan

[84] National and Kapodistrian University of Athens, School of Science, Department of Physics , Athens, Greece

[85] National Centre for Nuclear Research, Warsaw, Poland

[86] National Institute of Science Education and Research, Homi Bhabha National Institute, Jatni, India

[87] National Nuclear Research Center, Baku, Azerbaijan

[88] National Research Centre Kurchatov Institute, Moscow, Russia

[89] Niels Bohr Institute, University of Copenhagen, Copenhagen, Denmark

[90] Nikhef, National institute for subatomic physics, Amsterdam, Netherlands

[91] NRC Kurchatov Institute IHEP, Protvino, Russia

[92] NRC "Kurchatov" Institute — ITEP, Moscow, Russia

[93] NRNU Moscow Engineering Physics Institute, Moscow, Russia

[94] Nuclear Physics Group, STFC Daresbury Laboratory, Daresbury, United Kingdom

[95] Nuclear Physics Institute of the Czech Academy of Sciences, Řež u Prahy, Czech Republic

[96] Oak Ridge National Laboratory, Oak Ridge, Tennessee, United States

[97] Ohio State University, Columbus, Ohio, United States

[98] Petersburg Nuclear Physics Institute, Gatchina, Russia

[99] Physics department, Faculty of science, University of Zagreb, Zagreb, Croatia

[100] Physics Department, Panjab University, Chandigarh, India

[101] Physics Department, University of Jammu, Jammu, India

[102] Physics Department, University of Rajasthan, Jaipur, India

[103] Physikalisches Institut, Eberhard-Karls-Universität Tübingen, Tübingen, Germany

[104] Physikalisches Institut, Ruprecht-Karls-Universität Heidelberg, Heidelberg, Germany

105 *Physik Department, Technische Universität München, Munich, Germany*
106 *Politecnico di Bari, Bari, Italy*
107 *Research Division and ExtreMe Matter Institute EMMI, GSI Helmholtzzentrum für Schwerionenforschung GmbH, Darmstadt, Germany*
108 *Rudjer Bošković Institute, Zagreb, Croatia*
109 *Russian Federal Nuclear Center (VNIIEF), Sarov, Russia*
110 *Saha Institute of Nuclear Physics, Homi Bhabha National Institute, Kolkata, India*
111 *School of Physics and Astronomy, University of Birmingham, Birmingham, United Kingdom*
112 *Sección Física, Departamento de Ciencias, Pontificia Universidad Católica del Perú, Lima, Peru*
113 *St. Petersburg State University, St. Petersburg, Russia*
114 *Stefan Meyer Institut für Subatomare Physik (SMI), Vienna, Austria*
115 *SUBATECH, IMT Atlantique, Université de Nantes, CNRS-IN2P3, Nantes, France*
116 *Suranaree University of Technology, Nakhon Ratchasima, Thailand*
117 *Technical University of Košice, Košice, Slovakia*
118 *The Henryk Niewodniczanski Institute of Nuclear Physics, Polish Academy of Sciences, Cracow, Poland*
119 *The University of Texas at Austin, Austin, Texas, United States*
120 *Universidad Autónoma de Sinaloa, Culiacán, Mexico*
121 *Universidade de São Paulo (USP), São Paulo, Brazil*
122 *Universidade Estadual de Campinas (UNICAMP), Campinas, Brazil*
123 *Universidade Federal do ABC, Santo Andre, Brazil*
124 *University of Cape Town, Cape Town, South Africa*
125 *University of Houston, Houston, Texas, United States*
126 *University of Jyväskylä, Jyväskylä, Finland*
127 *University of Liverpool, Liverpool, United Kingdom*
128 *University of Science and Technology of China, Hefei, China*
129 *University of South-Eastern Norway, Tonsberg, Norway*
130 *University of Tennessee, Knoxville, Tennessee, United States*
131 *University of the Witwatersrand, Johannesburg, South Africa*
132 *University of Tokyo, Tokyo, Japan*
133 *University of Tsukuba, Tsukuba, Japan*
134 *Université Clermont Auvergne, CNRS/IN2P3, LPC, Clermont-Ferrand, France*
135 *Université de Lyon, Université Lyon 1, CNRS/IN2P3, IPN-Lyon, Villeurbanne, Lyon, France*
136 *Université de Strasbourg, CNRS, IPHC UMR 7178, F-67000 Strasbourg, France, Strasbourg, France*
137 *Université Paris-Saclay Centre d'Etudes de Saclay (CEA), IRFU, Départment de Physique Nucléaire (DPhN), Saclay, France*
138 *Università degli Studi di Foggia, Foggia, Italy*
139 *Università degli Studi di Pavia, Pavia, Italy*
140 *Università di Brescia, Brescia, Italy*
141 *Variable Energy Cyclotron Centre, Homi Bhabha National Institute, Kolkata, India*
142 *Warsaw University of Technology, Warsaw, Poland*
143 *Wayne State University, Detroit, Michigan, United States*
144 *Westfälische Wilhelms-Universität Münster, Institut für Kernphysik, Münster, Germany*
145 *Wigner Research Centre for Physics, Budapest, Hungary*
146 *Yale University, New Haven, Connecticut, United States*
147 *Yonsei University, Seoul, Republic of Korea*